Fernández-Guisuraga *et al. Fire Ecology* (2025) 21:30
https://doi.org/10.1186/s42408-025-00373-4

Fire Ecology

ORIGINAL RESEARCH

Open Access

Estimation of Prometheus fuel types using physically based remote sensing techniques

José Manuel Fernández-Guisuraga[1,2,3*], Andrea Monzón-González[1], Víctor Fernández-García[4], Sergio Alberto Peña-Pérez[5] and Leonor Calvo[1,6]

Abstract

Background Detailed knowledge of the spatial distribution of vegetation fuels is essential for assessing wildfire hazard and behavior, as well as for planning effective management. In southern Europe, the Prometheus project has proposed the differentiation of seven fuel types, but their characterization using remote sensing techniques remains challenging. Here, we propose a two-phase, innovative methodology for high-resolution mapping of Prometheus fuel types, integrating complementary remote sensing data and physically based techniques. In the first phase, we estimated the fire-propagating element (grass, shrubs, and trees) through multispectral imagery and an advanced spectral unmixing technique (multiple endmember spectral mixture analysis—MESMA) to mimic the Prometheus classification system in the field. In the second phase, synthetic aperture radar data, together with a novel LiDAR workflow related to the distribution of leaf area density by fuel vertical strata, were used to classify the corresponding Prometheus fuel type (FT) within each fire-propagating element (grassland, shrubland, and woodland) by using a random forest classification algorithm.

Results Field validation conducted across four sites in the Iberian Peninsula with markedly different environmental conditions and vegetation types showed high performance in the classification of the fire-propagating element through MESMA (overall accuracy (OA) = 94.58%). The producer's (PA) and user's (UA) accuracy for each class (> 90.00%) was consistent with the OA. During the second phase, fuel types in shrublands (FT2 to FT4) and woodlands (FT5 to FT7), together with the fuel type in grasslands (FT1) retrieved directly from MESMA, were classified with high overall performance (OA = 90.27%) as depicted by the validation of the final Prometheus fuel type map from a set of independent field plots. The PA and UA for most individual FTs exceeded 80%.

Conclusions The results of this manuscript provide an accurate characterization of the spatial variability of fuel types within the Prometheus classification system across heterogeneous landscapes. The generalizability of the remote sensing methodology proposed, grounded in physical and ecological principles, represents a significant advance for fuel planning in southern European countries.

Keywords LiDAR, Mediterranean Basin, MESMA, Random forest, SAR, Sentinel-2

Resumen

Antecedentes El conocimiento detallado de la variabilidad espacial de los combustibles vegetales es esencial para determinar el riesgo y comportamiento de los incendios forestales, como así también para planificar estrategias de gestión efectivas. En el sur de Europa, el proyecto Prometheus ha propuesto la diferenciación de siete tipos de

*Correspondence:
José Manuel Fernández-Guisuraga
jofeg@unileon.es
Full list of author information is available at the end of the article

combustibles, aunque su caracterización mediante el uso de técnicas de teledetección resulta todavía desafiante. En este trabajo, proponemos una metodología innovadora, en dos fases, para el mapeo en alta resolución de los tipos de combustible Prometheus, integrando datos de teledetección complementarios y técnicas con base física. En la primera fase, estimamos los elementos propagadores del fuego (pasto, matorral, y árboles) a través de imágenes multiespectrales y una técnica de mezclas espectrales avanzada (*multiple endmember spectral mixture analysis -MESMA-*) para imitar la clasificación del sistema Prometeus en campo. En la segunda fase, usamos datos de radar de apertura sintética junto con un flujo de trabajo LIDAR novedoso, relacionado con la estimación de la distribución de la densidad del área foliar y los estratos verticales del combustible, para clasificar el correspondiente tipo de combustible del Prometheus (FT) dentro de cada elemento propagador del fuego, usando el algoritmo de clasificación Random Forest.

Resultados La validación en campo realizada a través de cuatro sitios de estudio en la Península Ibérica, con marcadas diferencias en sus condiciones ambientales y tipos de vegetación, mostraron un alto rendimiento en la clasificación de los elementos de propagación del fuego a través de MESMA (precisión global o *overall accuracy* -OA- = 94.58%). La precisión del Productor (PA) y del Usuario (UA) para cada clase (> 90.00%) fue consistente con la OA. Durante la segunda fase, los tipos de combustibles de matorral (FT2 a FT4) y de arbolado (FT5 a FT7), junto con el tipo de combustible de pasto (FT1), estimado directamente de MESMA, fueron clasificados con un alto rendimiento (OA = 90.27%) como muestra en la validación final del mapa de tipos de combustible Prometheus a partir de un conjunto de parcelas de campo independientes. La PA y UA de cada FT excedió el 80%.

Conclusiones Los resultados de este trabajo proporcionan una metodología para clasificar de forma precisa la variabilidad espacial de los tipos de combustibles dentro del sistema Prometheus a través de diferentes tipos de paisaje. La generalización de la metodología de teledetección propuesta, basada en principios físicos y ecológicos, representa un avance significativo para la planificación de las estrategias de gestión del combustible en los países del sur de Europa.

Introduction

Wildfires have become an increasingly global threat, driven by the interaction of climatic, ecological, and human factors, resulting in significant socio-economic and environmental resources losses (Abdollahi & Yebra 2023). Terrestrial ecosystems in the Mediterranean Basin are highly vulnerable to wildfire disturbances due to their seasonal climate and the presence of highly flammable biomass (Moreira et al. 2011; San Miguel-Ayans et al., 2013). These conditions, aggravated by rural land abandonment and climate change, have led to a high buildup and continuity of dry, flammable fuels conducive to fire ignitions and extreme fire behavior (Moritz et al. 2012; Pausas & Keeley 2021; Hoffrén et al. 2024). The increasing occurrence of extreme wildfires has raised concerns about the effectiveness of current management and prevention strategies to address the hazard posed by altered fire regimes (Moritz et al. 2014).

Fuel load and structure across the landscape are the only components of the fire behavior triangle that managers can actively manipulate—unlike fire weather and topography—to minimize the ecological impacts of wildfires, i.e., fire severity (Fernández-García et al. 2022), and to reduce the potential loss of biodiversity, ecosystem functions, and services (Keeley et al. 2011; Hakkenberg et al. 2024). In this regard, accurate characterization of the spatial variability of fuel types in fire-prone landscapes is critical for modeling fire behavior (Martin-Ducup et al. 2025). Fuel biophysical properties and structural characteristics are summarized within the concept of fuel types (FTs), serving as classification systems that group plant community types with similar combustion and fire behavior patterns (Pyne et al. 1996; Benali et al. 2017). Fuel models, on the other hand, are specific numerical descriptions of FTs that include parameters necessary for calculating key fire behavior variables, such as rate of spread and fire intensity (Rothermel 1972). These parameters include fuel particle size, load, height, and bulk density (Aragoneses et al. 2023). Several FT classification systems have been proposed, with the most commonly used developed in the USA and Canada, such as those by Anderson (Anderson, 1982), the Northern Forest Fire Laboratory (NFFL) classification by Albini (Albini 1976), and the Canadian Forest Fire Behavior Prediction (FBP; Van Wagner et al. 1992). In Europe, researchers have developed a new fuel classification system called Prometheus (European Commission, 1999), which simplifies and adapts the NFFL classification based on Rothermel's fire spread model (Rothermel 1972) to the specific conditions of southern European ecosystems. The Prometheus system classifies fuels primarily by the type and height of the fire-propagating element (grass,

shrubs and trees), and divides them into seven FTs: grasslands (FT1), shrublands (FT2, FT3, FT4), and woodlands (FT5, FT6, FT7).

The characterization of the spatial variability of FTs has been mainly addressed through three approaches: (i) field surveys, (ii) photointerpretation of aerial imagery obtained via photogrammetry workflows combined with field data, and, more recently, (iii) through the analysis of optical data and active sensors onboard satellites or airplanes (Oswald et al. 1999; Chuvieco et al. 2003; Huesca et al. 2019; Viedma et al. 2020; Gale et al. 2021). Among these, remote sensing techniques have been established as a key tool in fuel assessments, enabling cost-effective observations and expanding their applicability in remote regions (Zhang et al. 2016; Gale et al. 2021). In contrast, methods based exclusively on field data and/or photointerpretation are costly, time consuming, present a limited spatial representativeness for the analysis of large areas (Viedma et al. 2020; Chamberlain et al. 2021), and do not capture fuel dynamics over time (Aragoneses & Chuvieco 2021). Several studies have implemented multispectral or hyperspectral satellite data with moderate-to-high spatial resolution, linked to geographic information systems, to capture the spatial variability of plant communities, plant species or, more specifically, of FTs through pixel or object-based analyses (e.g., Arroyo et al. 2006; Mallinis et al. 2014; Hościło & Lewandowska 2019). However, such data may perform suboptimally when characterizing understory fuels and vertical fuel continuity under dense canopy cover (Jakubowksi et al. 2013; Marino et al. 2016). The estimation of these fuel parameters, together with vegetation height, which are essential variables for distinguishing FTs and predicting fire behavior (Benali et al. 2017), often relies on indirect correlations with optical signals.

This limitation can be overcome by active sensors such as light detection and ranging (LiDAR) and synthetic aperture radar (SAR) (Gale et al. 2021). Airborne LiDAR technology allows accurate characterization of three-dimensional fuel structure across large areas (Hummel et al. 2011; Chamberlain et al. 2021), even with low point cloud density datasets by leveraging an area-based approach (Fernández-Guisuraga et al. 2022a). Indeed, low-density LiDAR data are anticipated to offer superior insights into understory fuel structure compared to satellite-based multispectral or hyperspectral observations (Morsdorf et al. 2006). Previous studies have shown that LiDAR can accurately capture relevant fuel structural attributes, including canopy base height (Engelstad et al. 2019), canopy bulk density (Chamberlain et al. 2021), canopy volume (Næsset et al., 2005), vegetation height (Valbuena et al. 2017), and structure classes (Moran et al. 2018), among others. Microwave backscatter data, such as those provided by the C-band SAR sensor onboard Sentinel-1, can provide reliable insights about the density and size distribution of stems, foliage, and branches in the canopy (Patenaude et al., 2005), providing information about the vertical fuel structure complementary to LiDAR data (Fernández-Guisuraga et al. 2023a, b). However, the potential of SAR data for mapping FTs remains to be thoroughly explored (Solares-Canal et al. 2023).

Previous studies have leveraged the fusion of multispectral data with LiDAR point clouds to capture the spatial variability of FTs in southern European countries using decision rules and/or machine learning algorithms (García et al. 2011; Marino et al. 2016; Domingo et al. 2020; Solares-Canal et al. 2023; Hoffrén et al. 2024). For instance, García et al. (2011) implemented a two-phase classification approach where a support vector machine algorithm was first used to hard-classify the fire-propagating element within the Prometheus system from high-resolution, airborne multispectral imagery in central Spain. This initial classification served as the foundation for a subsequent decision rule to assign FTs within each fire-propagating element by means of LiDAR data. The same procedure was leveraged by Solares-Canal et al. (2023) to classify Rothermel FTs in northwest Spain. Domingo et al. (2020) used a single-phase approach to directly classify FTs within the Prometheus system using Sentinel-2 multispectral data and LiDAR point clouds in eastern Spain. The methods implemented in these studies are based, in some of their stages, on a hard-classification of remotely sensed data to estimate the fire-propagating element or directly the FT at the pixel level.

The distinction in the field of the fire-propagating element in the Prometheus system is based on percentages of grass, shrub, and tree fractional cover (see section "Field sampling of fuel types") (European Commission, 1999). In homogeneous areas, a hard-classification approach may adequately adhere to the decision rules of the Prometheus system. However, in landscapes with high spatial heterogeneity within fire-propagating elements, this method may misclassify pixels by assigning them to the dominant endmember, even when its percentage cover is as low as 30% (Fernández-García et al. 2021; Fernández-Guisuraga et al. 2024a). Moreover, hard-classifications lack physical significance, and while this has not yet been thoroughly evaluated, the generality and transferability of FT estimates are likely limited between landscapes dominated by dissimilar plant communities and with distinct environmental conditions (Feilhauer & Schmidtlein 2011). The retrieval of image fractions at sub-pixel level through spectral unmixing techniques can thus be a more robust alternative adapted to the Prometheus system. Spectral mixture analysis (SMA) has been widely implemented in the fire ecology field for

assessing fire severity (Quintano et al. 2013, 2023) or ecosystem resilience (Fernández-Guisuraga et al. 2020). Particularly, multiple Endmember Spectral Mixture Analysis (MESMA; Roberts et al. 1998) is an advanced spectral unmixing technique specifically designed to account for spectral variability within each endmember of interest (Dennison & Roberts 2003), such as the fire-propagating elements in Prometheus. This technique enables the incorporation of multiple spectra for each endmember and decomposes the reflectance signal of each pixel using various combinations of potential endmembers. This approach overcomes a key limitation of traditional SMA-based algorithms, which require a fixed number of endmembers to unmix each pixel, regardless of whether those endmembers are actually represented within the pixel (Quintano et al. 2013). Although MESMA has not yet been applied to FT mapping, it provides a more physically meaningful approach with greater potential for estimating cover fractions of fire-propagating elements compared to conventional hard-classification methods. Moreover, recent advancements by Kamoske et al. (2019) and Viedma et al. (2024) introduced workflows leveraging LiDAR data to examine the distribution of the leaf area density (LAD) across vertical fuel layers. These methods provide critical insights into both horizontal and vertical fuel continuity, including the identification of fuel gaps and the characterization of fuel layer depth within forest stands. However, these approaches remain unexplored in the context of FT mapping.

Several studies have emphasized the need to evaluate remote sensing-based approaches for mapping FTs at broad spatial scales to account for their potential under highly variable environmental conditions and diverse plant community types (Marino et al. 2016; Solares-Canal et al. 2023), as well as their applicability in decision-making processes (Cardil et al. 2021). In this manuscript, the fusion of multispectral, LiDAR, and SAR data, as well as physically based remote sensing techniques, is proposed to characterize the spatial variability of FTs within the Prometheus system using a two-phase classification method across four extensive study sites. These sites encompass a high diversity of plant community types and are located along an Atlantic-Mediterranean climatic gradient in the Iberian Peninsula. In the first phase, the MESMA algorithm is applied for the first time to classify fire-propagating elements from Sentinel-2 scenes by mimicking the Prometheus decision rules in the field. In the second phase, a machine learning algorithm is trained to assign FTs within each propagating element by leveraging (i) novel voxel-based LiDAR metrics accounting for fuel density and LAD distribution across vertical strata, (ii) the fractional vegetation cover (FCOVER) retrieved from Sentinel-2 scenes, and (iii) a cross-polarization ratio of C-band SAR (Sentinel-1) backscatter data (SAR-CR) indicative of vegetation density and structural complexity. The proposed method was validated with an independent set of field plots across all study sites. The ecological and physical foundation of our approach aims to improve the estimation and classification of FTs in fire-prone ecosystems, offering a more generalizable tool for fire behavior modeling and fire risk management.

Material and methods

Study sites

The study sites are located within an Atlantic-Mediterranean climatic gradient in the Iberian Peninsula (Fig. 1).

Bejís site is located in the Sierra de Andilla mountain range (eastern Iberian Peninsula) and covers an extension of 83,125 ha. The topography of the site is rugged, with prominent slopes. The altitude ranges between 550 and 1600 m. Climate is Mediterranean, with more than 3 months of summer drought. The mean annual precipitation is 560 mm, and the mean annual temperature 15 °C (Ninyerola et al. 2005). The site is dominated by *Pinus halepensis* Mill., *P. pinaster* Ait. and *P. nigra* Arnold forests, *Quercus ilex* L. woodlands, and *Q. coccifera* L., *Ulex parviflorus* Pourr., *Genista scorpius* (L.) DC, and *Juniperus oxycedrus* L. shrublands.

Culebra site is located in the Sierra de la Culebra mountain range (northwestern Iberian Peninsula). The study site covers 67,910 ha and is located at the transition between Mediterranean and Atlantic climatic regions. The region is characterized by 3 months of summer drought, with a mean annual temperature of 11 °C and a mean annual precipitation of 750 mm (Ninyerola et al. 2005). The topography is characterized by steep hillsides and broad valleys, with elevations ranging from 750 to 1200 m. Plant communities are dominated by *P. pinaster*, *P. sylvestris*, and *Q. pyrenaica* Willd. forests, *Q. ilex* L. woodlands, together with shrublands of *Pterospartum tridentatum* (L.) Willk, *Cistus ladanifer* L., *Halimium lasianthum* subsp. *alyssoides* (Lam.) Greuter and *Erica australis* L., and Mediterranean grasslands.

Folgoso site is located within the Sierra do Courel mountain range (northwestern Iberian Peninsula) and covers an extension of 62,430 ha. The site has very complex topographic conditions, with prominent crests and narrow valley bottoms in the northeastern side, and moderate slopes with wide valleys on the southwestern side. The altitude ranges between 400 and 1600 m. The climate has predominant Atlantic characteristics, with mean annual precipitation and temperature of 1700 mm and 10 °C, respectively (Ninyerola et al. 2005). Vegetation types include mixed forests dominated by *Castanea sativa* Mill., *Q. pyrenaica* and *Fagus sylvatica* L., *P.*

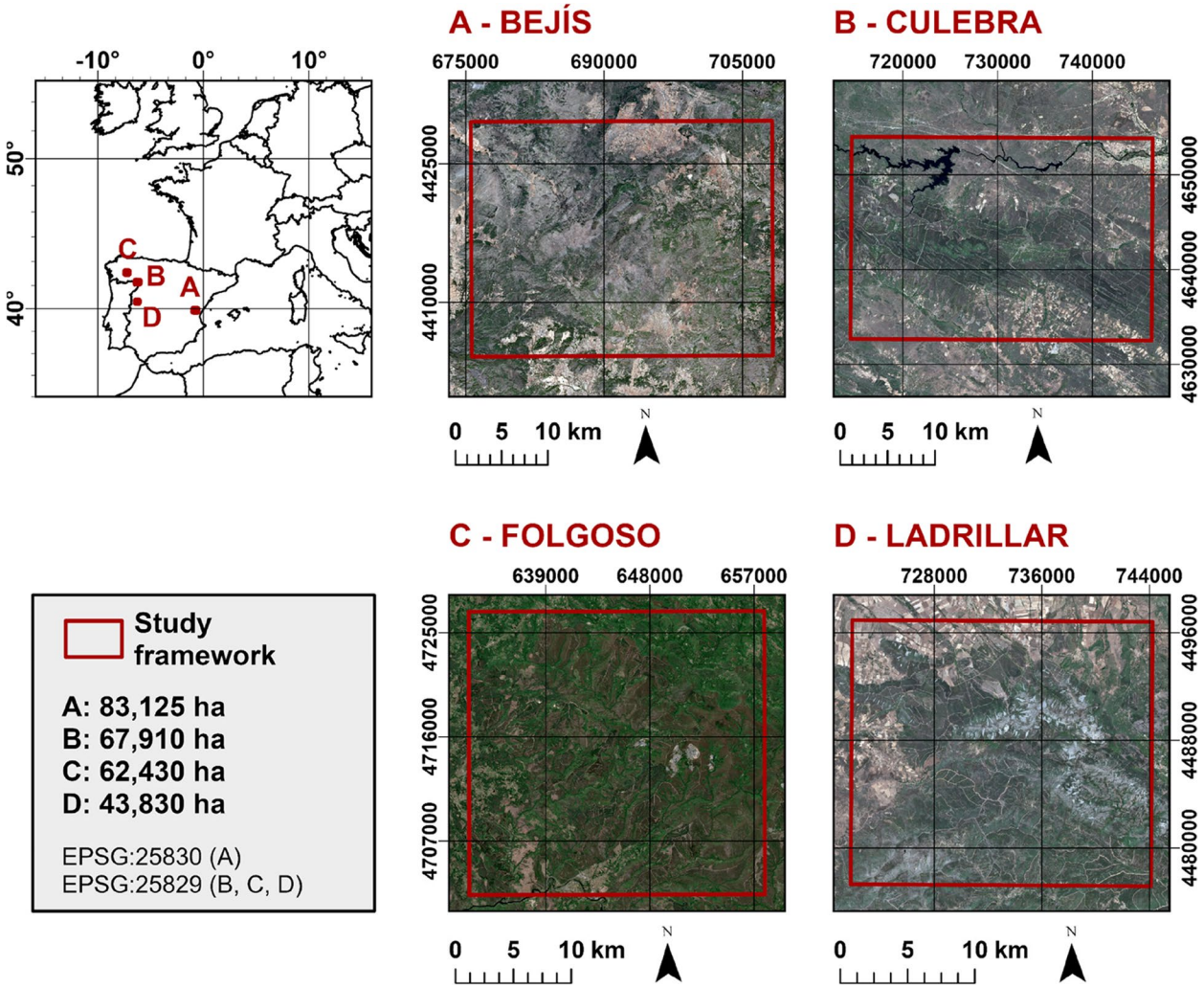

Fig. 1 Location of the study sites along an Atlantic-Mediterranean climatic gradient in the Iberian Peninsula

pinaster and *P. sylvestris* forests, *Q. ilex* and *Q. suber* L. woodlands, and shrublands dominated by *E. australis*, *U. europaeus* L. and *Cytisus scoparius* (L.) Link.

Ladrillar site occupies 43,830 ha and is located between the Sierra de Gata and the Sierra de Francia mountain ranges (central-western Iberian Peninsula), with altitudes ranging between 400 and 1300 m. The site has a rugged topography with steep hillsides and wide valleys. The climate is Mediterranean, with more than 3 months of summer drought. The mean annual temperature is 13 °C and the mean annual precipitation 1000 mm. The dominant vegetation consists of *P. sylvestris* and *P. pinaster* forests, *Q. ilex* woodlands, and shrublands of *E. australis, C. ladanifer* and *P. tridentatum*.

Field sampling of fuel types

Between June and August 2024, a total of 215 plots of 20 m× 20 m were established in the field following the Sentinel-2 pixel grid to identify the FT according to the Prometheus criteria described in Fig. 2. The plots were randomly distributed throughout the study sites within structurally homogeneous areas of each fire-propagating element (i.e., grass, shrub, and tree), located beforehand with the aid of the Spanish Forest Map at 1:25,000 (SFM25) derived from the fourth Spanish National Forest Inventory (Alberdi et al. 2016). The number of plots within each fire propagating element (grass =34, shrub =70, tree =111) was carefully chosen to ensure a balanced representation of each class in the validation data partition (see section "Assignment of Prometheus fuel types and validation") and considering the area occupied by each of them within the study sites. We ensured a minimum distance of 200 m between plots, which were georeferenced using a GPS receiver in RTK mode. Four subplots of 2 m ×2 m were established within each plot, where all field measurements were conducted. For each

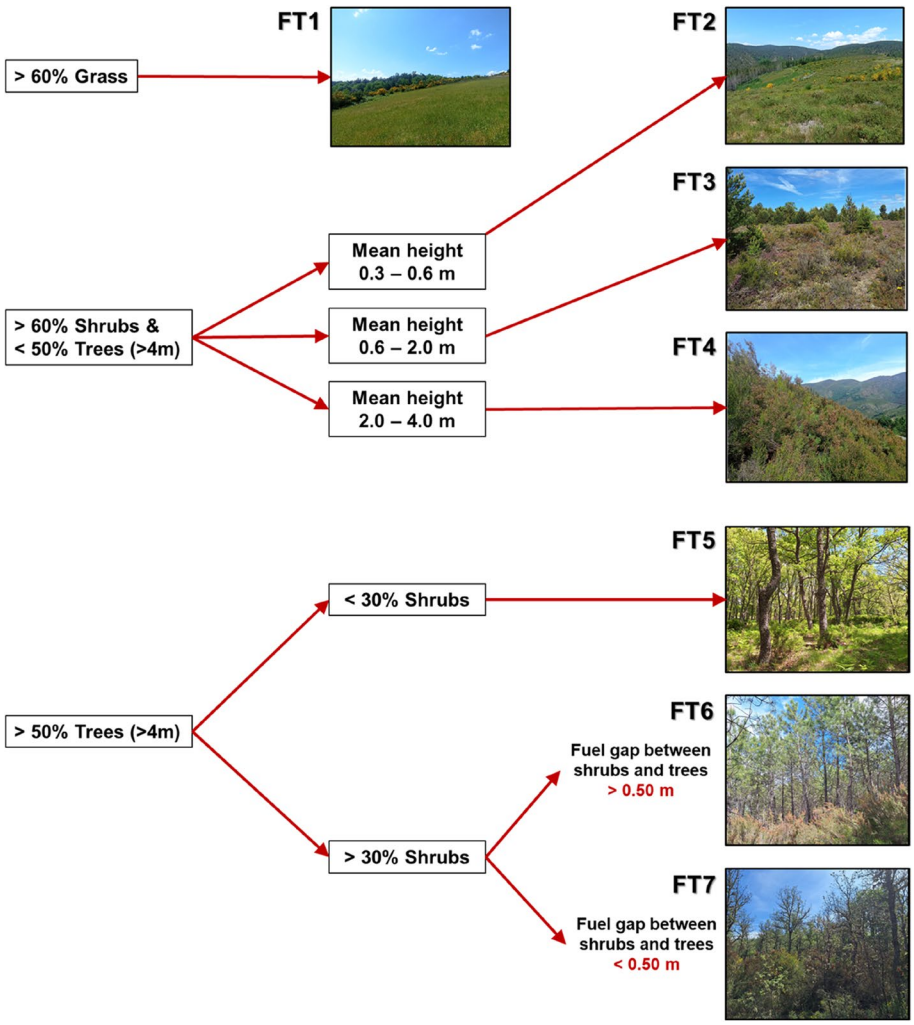

Fig. 2 Prometheus classification system and criteria for identification of fuel types (FTs) in the field (adapted from Riaño et al. 2002)

variable, the final value for the plot was calculated as the average of the values recorded in each subplot. The measured variables included (i) grass cover (%), (ii) shrub cover (%), (iii) tree cover (%), (iv) mean shrub height (m), (v) mean tree height (m), (vi) canopy base height (m), (vii) gap between canopy base and understory fuels (fuel gap; m), and (viii) total vegetation cover (%) in the vertical strata of < 0.3 m, 0.3–0.6 m, 0.6–2 m, 2–4 m, and > 4 m. Based on these measurements, the Prometheus FT was assigned for each plot.

Remote sensing data and processing

A workflow clarifying the methods used in this study is shown in Fig. 3. It includes field and remote sensing data collection, remote sensing data processing, and data analysis. The predictors of Prometheus FTs, derived from remote sensing data and techniques, are indicated in Table 1.

Remote sensing-derived products

The estimation of the Prometheus FTs (Fig. 2) for each framework within the study sites integrated several remote sensing datasets: (i) Sentinel-2 multispectral imagery and (ii) Sentinel-1 C-band SAR data from the Copernicus program of the European Space Agency (ESA), as well as (iii) LiDAR data provided by the Spanish National Plan for Aerial Orthophotography (PNOA).

Sentinel-2 Level-2 A surface reflectance data, atmospherically corrected and with a spatial resolution of 20 m, were acquired through the Google Earth Engine (GEE) platform ("COPERNICUS/S2_SR_HARMONIZED"product). The scenes were selected using a single-date approach, prioritizing the acquisition date closest to the field sampling date in each site and free of invalid pixels defined as clouds, haze, cloud shadows, or acquisition errors, as indicated by the Sentinel-2 quality band (QA60) and the GEE s2cloudless product. In cases where these conditions were

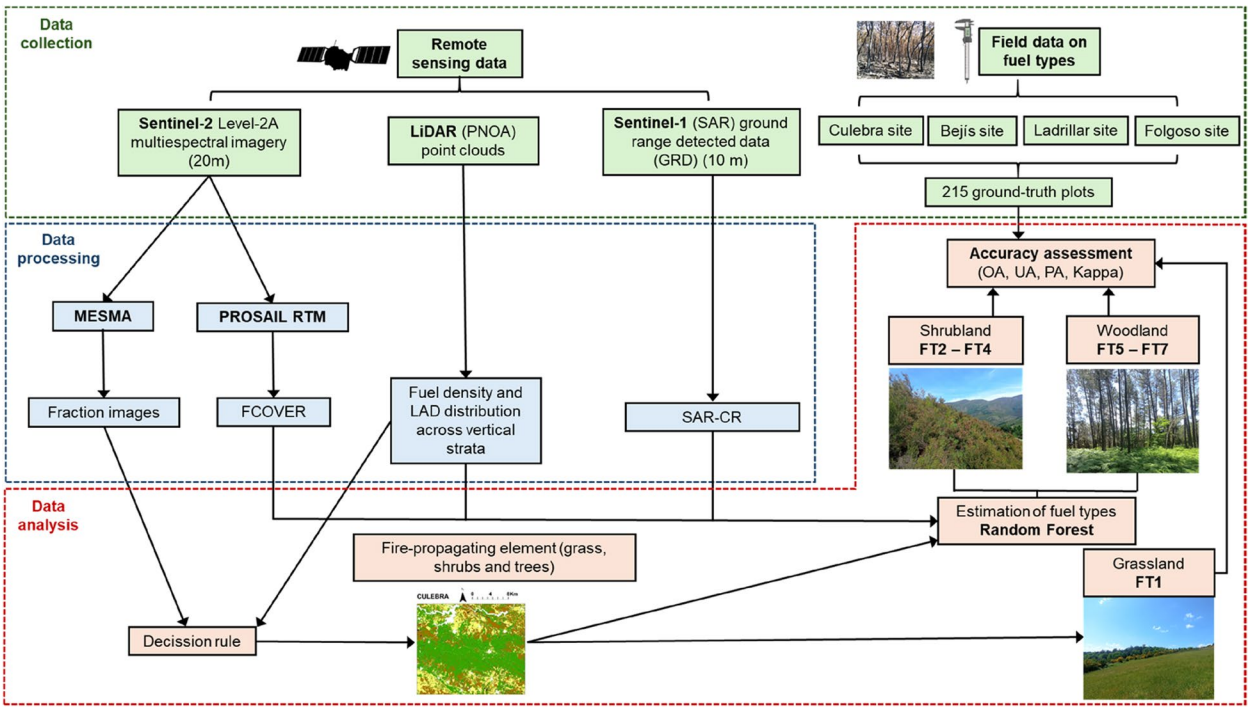

Fig. 3 Flowchart depicting field and remote sensing data collection, remote sensing data processing and data analysis

Table 1 Remote sensing-derived variables used as predictors of Prometheus fuel types (FTs) in this study

Source	Variable	Abbreviation	Unit
Sentinel-2	Fractional vegetation cover	FCOVER	%
Sentinel-1	SAR cross-polarization ratio	SAR-CR	-
PNOA LiDAR	Point cloud density < 0.3 m	$D_{<0.3\,m}$	%
	Point cloud density 0.3–0.6 m	$D_{0.3–0.6\,m}$	%
	Point cloud density 0.6–2 m	$D_{0.6–2\,m}$	%
	Point cloud density 2–4 m	$D_{2–4\,m}$	%
	Point cloud density > 4 m	$D_{>4\,m}$	%
	95 th percentile height of the returns	p95	m
	Vertical complexity index	VCI	-
	Leaf area index	LAI	$m^2\ m^{-2}$
	Maximum LAD	LAD_{MAX}	$m^2\ m^{-3}$
	Height of maximum LAD	LAD_{MAXH}	m
	Standard deviation of LAD	LAD_{STD}	$m^2\ m^{-3}$
	Volume of empty voxels	VOX_{EMPTY}	m^3
	Canopy rugosity	C_{RUG}	-
	Volume of the euphotic zone	$EUPH_V$	m^3
	Total leaf area in the euphotic zone	$EUPH_{LA}$	m^2
	Depth of the euphotic zone	$EUPH_D$	m
	Volume of the oligophotic zone	$OLIG_V$	m^3
	Total leaf area in the oligophotic zone	$OLIG_{LA}$	m^2

not met, a median composite from a maximum range of 30 days around the field sampling date ensured high-quality acquisitions.

In addition to the retrieval of fraction images of each fire propagating-element using MESMA (see section "Characterization of the fire-propagating element"), Sentinel-2 data were used to estimate the fractional vegetation cover (FCOVER; %), i.e., the top-of-canopy photosynthetic vegetation fraction observed from nadir, serving as a proxy for horizontal fuel continuity in both the canopy and understory where sensed through canopy gaps (Fernández-Guisuraga et al. 2021a). The FCOVER was retrieved from the inversion of the PROSAIL-D radiative transfer model (RTM) (Fernández-Guisuraga et al. 2021a, 2021b; Fernández-Guisuraga et al. 2023a, b). Remarkably, RTMs elucidate the mechanistic relationships between top-of-canopy reflectance and the variability in vegetation biophysical attributes, offering a robust physical and ecological foundation (Wang et al. 2022). As a result, RTMs demonstrate superior generalization capabilities across diverse plant community types compared to empirical models (Yebra & Chuvieco 2009). A comprehensive description of the parameterization, forward simulation, and inversion of the PROSAIL-D RTM is provided in Fernández-Guisuraga et al. (2021a, b).

C-band SAR data from the Sentinel-1 ground range detected (GRD) product, with a spatial resolution of 10

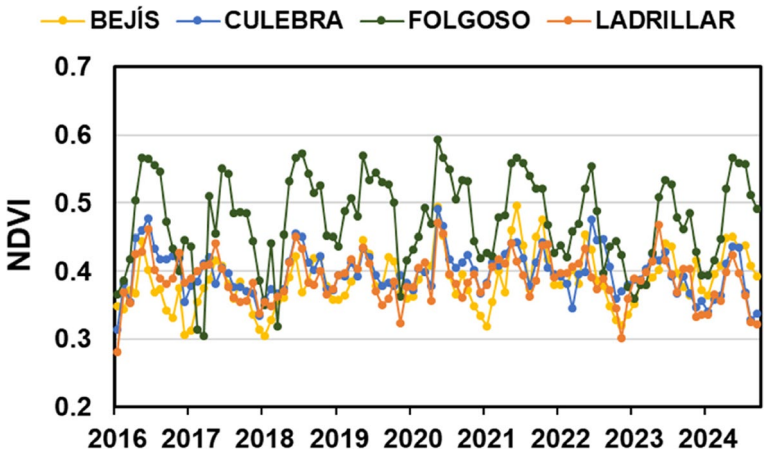

Fig. 4 Temporal trend of the normalized difference vegetation index (NDVI) for each field plot in the study sites between January 2016 and September 2024

m, were acquired via the GEE platform ("COPERNICUS/S1_GRD"product). Scene selection was based on their temporal proximity to the field sampling dates, ensuring no precipitation occurred within the 7 days prior to each acquisition. This criterion was established due to the sensitivity of C-band SAR backscatter behavior to variations in soil and vegetation moisture, which can obscure the influence of vegetation structure (Belenguer-Plomer et al. 2019). The condition was verified using the ERA5-Land Daily Aggregated product from the ECMWF Climate Reanalysis, available on GEE ("ECMWF/ERA5_LAND/DAILY_AGGR"product). The SAR cross-polarization ratio (SAR-CR) was derived from backscatter data of VH and VV polarizations of the Sentinel-1 GRD product (Meyer 2019). This metric can complement LiDAR data for characterizing the spatial variability of vegetation density and the structural complexity of plant communities (Fernández-Guisuraga et al. 2024).

LiDAR data were collected between 2017 and 2021 in the study sites with a mean density of 2–4 points m^{-2} and a vertical accuracy ($RMSE_Z$) of the point cloud less than 0.2 m as reported by PNOA. Although there is a temporal gap between LiDAR acquisition and the field sampling dates (June–August 2024), LiDAR data were considered representative of the fuel type and structure prior to sampling, as no significant natural or anthropic disturbances were identified between both dates. This was confirmed based on the temporal trend of the normalized difference vegetation index (NDVI) calculated from monthly composites of valid pixels from Sentinel-2 Level-1 C data in Google Earth Engine (GEE) for each field plot in the study sites between January 2016 and September 2024. No abrupt changes in NDVI were observed throughout the time series beyond the intra-annual variability associated with the phenology of the species (Fig. 4).

To classify the LiDAR point clouds into ground and non-ground returns, several algorithms were evaluated: (i) the Multiscale Curvature Classification (MCC; Evans & Hudak 2007), (ii) the Progressive Morphological Filter (PMF; Zhang et al. 2003) and (iii) the Cloth Simulation Filter (CSF; Zhang et al. 2016) using the lidR package (Roussel et al. 2020) in R (R Core Team 2023), as well as (iv) a progressive triangulated irregular network (TIN) densification algorithm (Axelsson 2000) implemented in LAStools (rapidlasso GmbH, Germany). Since these algorithms require extensive parameterization to maximize accuracy in areas with varying vegetation types, topography, and soil patchiness, multiple batch runs were conducted with different input parameters. The performance of each algorithm was evaluated visually by inspecting the classified point clouds in heterogeneous test areas against high-resolution RGB orthophotographs (20–50 cm) from PNOA. This widely adopted approach is recommended for parameterizing and evaluating the performance of LiDAR ground filtering algorithms (Hillman et al. 2021; Fernández-Guisuraga et al., 2024b). Ultimately, the progressive TIN algorithm from LAStools was selected and executed in the lowest points of a 5-m grid.

Ground returns were interpolated to generate a digital terrain model (DTM) with a spatial resolution of 2 m. The DTM was used to normalize point cloud heights and subsequently calculate a set of common area-based LiDAR metrics with ecological relevance. The metrics were derived at a spatial resolution of 20 m × 20 m and aligned with the grid of Sentinel-2 Level-2 A scenes. The calculated metrics included the point cloud density (%) across height bin intervals

($D_{<0.3\ m}$, $D_{0.3–0.6\ m}$, $D_{0.6–2\ m}$, $D_{2–4\ m}$, and $D_{>4\ m}$) to represent the vertical distribution of fuels by mimicking the strata of the Prometheus system for plots dominated by shrubs or trees as the primary fire-propagating element. Density metrics were calculated as the proportion of returns within a specific stratum relative to the total number of aboveground returns (Woods et al. 2011). The 95 th percentile height of the returns (p95; m) was used as an estimate of the canopy height in the grid (Kwak et al. 2014). The vertical complexity index (VCI) proposed by van Ewijk et al. (2011) was derived using uniform 0.5-m height bins to evaluate the evenness of fuel distribution along the vertical profile (Fernández-Guisuraga et al. 2022a). Lastly, a canopy height model (CHM) with the same grid size as that of the DTM (2 m) was calculated from the interpolation of the highest normalized LiDAR returns with a TIN (Fernández-Guisuraga et al. 2022a), to be included in the decision rule for the classification of the fire-propagating element (see Sect. 2.3.2) and assist in distinguishing between shrub and tree (Woolley 2016) fire-propagating elements.

Additionally, we considered several LiDAR metrics not yet explored in the context of FT mapping and related to the LAD ($m^2\ m^{-3}$) distribution across vertical fuel layers. These metrics were calculated using the canopyLazR package (Kamoske et al. 2019) in R for 1-m deep voxels aligned to the Sentinel-2 grid. The LAD distribution may play a critical role in representing the horizontal and vertical arrangement of fuel within the stand, thus influencing potential fire behavior, such as crown fire initiation. Indeed, these metrics provide valuable insights into the vertical continuity of fuel layers (e.g., ladder fuels) as well as their fuel depth and spacing in the canopy (Viedma et al. 2024). Among the calculated metrics were the (i) leaf area index (LAI; $m^2\ m^{-2}$), (ii) maximum LAD (LAD_{MAX}; $m^2\ m^{-3}$), (iii) height of maximum LAD (LAD_{MAXH}; m), (iv) standard deviation of LAD (LAD_{STD}; $m^2\ m^{-3}$), (v) volume of empty voxels (VOX_{EMPTY}; m^3), (vi) canopy rugosity (C_{RUG}) as an indicator of LAD vertical heterogeneity (Hardiman et al. 2011), (vii) volume of the euphotic zone ($EUPH_V$; m^3), (viii) total leaf area in the euphotic zone ($EUPH_{LA}$; m^2), (ix) depth of the euphotic zone ($EUPH_D$; m), (x) volume of the oligophotic zone ($OLIG_V$; m^3), and (xi) total leaf area in the oligophotic zone ($OLIG_{LA}$; m^2). The euphotic zone comprises all filled voxels of the vertical profile that are within the uppermost 65% of plant material within the column (Lefsky et al. 1999; Kamoske et al. 2022), and thus may be representative of the density and continuity of canopy fuels. The oligophotic zone represents the bottommost 35% of plant material (Lefsky et al. 1999; Kamoske et al. 2022) and thus may be indicative of the density of understory and ladder fuels in the stand.

Characterization of the fire-propagating element

Two steps were followed to implement the MESMA procedure and retrieve the subpixel image fractions of each fire-propagating element in Prometheus from Sentinel-2 Level-2 A surface reflectance scenes.

The first phase of the MESMA procedure requires the extraction of endmember spectra that capture the inherent spectral variability of the plant communities within each fire-propagating element. In this work, endmember spectra were obtained through the Sentinel-2 image itself (i.e., image endmembers; Settle & Campbell 1998). The process began with the identification of candidate endmembers (spectra of land cover components) to construct a spectral library, which was subsequently used in the spectral unmixing process. A structured spectral library was developed at multiple hierarchical levels following Quintano et al. (2023). The most general level of the spectral library (level 1) comprised the fire-propagating element (non-fuel, grass, shrub, tree). For example, within forest communities, level 2 would include coniferous, broadleaf, or mixed stands, and within coniferous forests, level 3 would encompass endmember spectra of species such as *P. pinaster*, *P. sylvestris*, or *P. nigra*, among others. This hierarchical structure allows for the establishment of multiple levels of complexity, which can be applied concurrently to unmix the Sentinel-2 scene through a multilevel fusion approach (Roberts et al. 1998). This process was supported by orthophotographs from the PNOA, the SFM25, and true (B4-B3-B2) and false (B12-B8 A-B4) color composites of Sentinel-2 scenes. Spectral signatures were verified to ensure their correspondence with targeted land cover classes by expert knowledge (Quintano et al. 2020). The final set of candidate endmembers represented the variability of land cover types within the study sites, including the different types of non-fuel areas. The definitive spectral library was constructed using the Iterative Endmember Selection (IES) algorithm (Roth et al. 2012) to identify the most relevant endmembers that maximize the Kappa index to unmix Sentinel-2 scenes according to the fractional cover of fire-propagating elements (level 1) within each pixel. The allowable endmember fractions were constrained within a range of 0 to 1, while the maximum permissible root mean square error (RMSE) for the spectral unmixing process was limited to 0.025.

The second phase involved the spectral unmixing of Sentinel-2 scenes using a multi-level fusion procedure covering simultaneously several levels of complexity arising from the hierarchical organization of the definitive spectral library (Roberts et al. 2003). The MESMA

modeling process was iterative, adjusting the maximum number of endmembers considered in each model and optimizing their spectral signatures until the imposed constraints were met. These constraints included fraction values between 0 and 1, a maximum shadow fraction of 0.8, a maximum RMSE of 0.025, and no more than 5% of unclassified pixels (Quintano et al. 2013, 2023). Fraction images representing the subpixel cover of level 1 endmembers (non-fuel, grass, shrub, tree) were shade-normalized using the endmember derived from photometric shade. In addition to including a level 1 endmember representing non-fuel areas, a mask based on layers from the Spanish National Topographic Base was applied to the fraction images to reduce errors in identifying this land cover class. For further specification of the process, see the paper by Quintano et al. (2023).

We used a decision rule to assign each pixel to the dominant fire-propagating element by considering the MESMA fraction images and the variability of the LiDAR-derived CHM within each pixel of the fraction images. The assignment was made according to the established criteria in the Prometheus system (Fig. 2). Specifically, pixels with a grass cover fraction exceeding 0.6 were directly classified as the grass propagating element (FT1). If the shrub fraction was greater than 0.6 and the percentage of CHM pixels (2 m grid) higher than 4 m within each pixel of the MESMA fraction images (20 m grid) is less than 50%, the pixel was assigned to the shrub propagating element. Finally, we assigned the pixels with fuel taller than 4 m covering more than 50% of the landscape as the tree propagating element. This approach would presumably avoid most of the errors associated with the exclusive use of either multispectral data or a CHM for landscape segmentation in this context. The classification of the fire-propagating element of the Prometheus system was initially evaluated using all field plots ($n = 215$) as they have not been seen by the MESMA algorithm. An additional randomly selected set of 25 photointerpreted plots derived from PNOA orthophotographs, corresponding to non-fuel areas, were used in the validation process. From the confusion matrix, we calculated the overall accuracy (OA; %) and the Kappa index, as well as the producer's (PA; %) and the user's (UA; %) accuracy for each class.

The MESMA procedure was implemented in the Visualization and Image Processing for Environmental Research (VIPER) tools 2.1 software (Roberts et al. 2019).

Assignment of Prometheus fuel types and validation

After classifying the fire propagating element for each pixel in Sentinel-2 scenes, the specific assignment of each Prometheus FT within shrubland (FT2, FT3, FT4) and woodland (FT5, FT6, FT7) pixels was addressed. The FT1 model was directly assigned to the grass-type propagating element. We randomly selected 70% of the field plots in shrubland and woodland areas (training dataset) to calibrate an independent Random Forest (RF; Breiman 2001) classification algorithm for each fire propagating element pooling data from the four study sites following Marino et al. (2016). A stratified random sampling was used to ensure that the training and validation sets had approximately the same percentage of samples of each target class as the complete dataset. Therefore, two independent RF models were calibrated: one for plots in which the fire-propagating element was classified as shrub, and another for plots classified as tree. The categorical dependent variable was the FT of each field plot of the training dataset. Predictors, aggregated at the plot level (20 m × 20 m), were the FCOVER, SAR-CR, and LiDAR metrics, excluding the CHM. These variables were extracted by averaging data from a systematically distributed 20-m grid of points within each plot, spaced 2 m apart. This approach was designed to minimize potential discrepancies between the pixel grids and the actual boundaries of the field plots (Picotte & Robertson 2011).

The Boruta feature selection algorithm (Kursa & Rudnicki 2010), a wrapper method built around RF, was used in this study to minimize the dimensionality of predictors in each RF model, while enhancing model robustness and predictive performance (Speiser et al. 2019). Boruta evaluates variable importance using Z-scores derived from a holdout approach and classifies predictors as "unconfirmed," "tentative," or "confirmed" by comparing their importance against shadow variables (Kursa & Rudnicki 2010). The variables categorized as "confirmed" by Boruta were included in the final RF predictor subset. The optimal value for the RF mtry hyperparameter was determined through fivefold cross-validation, while the ntree hyperparameter was set to 2000 to ensure prediction stability (Probst & Boulesteix 2018). Each RF model object was then applied alongside raster layers of the predictors to generate wall-to-wall FT maps within each fire propagating element determined by MESMA. Finally, the FT maps for shrubland (FT2, FT3, FT4) and woodland (FT5, FT6, FT7) areas were merged with those for grassland areas (FT1) to procure the final FT maps for each study site. The remaining 30% of field plots in shrubland ($n = 21$) and woodland ($n = 33$) areas (independent validation dataset), along with the total number of grassland plots ($n = 34$), unseen by RF, were used to evaluate the map accuracy through a confusion matrix and the OA and the Kappa index, together with the PA and UA for each FT. The 25 photointerpreted non-fuel plots were also used in the independent validation process.

Table 2 Confusion matrix and accuracy metrics (OA = overall accuracy; PA = producer's accuracy; UA = user's accuracy) for the classification of the dominant fire-propagating element in the Prometheus system using as reference the pooled field plots from the four study sites (n = 215). An additional 25 photointerpreted plots, corresponding to non-fuel areas, were used in the validation process

Fire-propagating element		Reference data			
		Tree	**Shrub**	**Grass (FT1)**	**No-fuel**
Classified data	**Tree**	105	3	0	0
	Shrub	6	66	1	0
	Grass (FT1)	0	1	33	2
	No-fuel	0	0	0	23
	PA (%)	94.60	94.29	97.06	92.00
	UA (%)	97.22	90.41	91.67	100.00
	OA (%)	**Kappa**			
	94.58	0.92			

All analyses were implemented in R (R Core Team 2023) using the RandomForest (Liaw and Wiener 2002), Boruta (Kursa & Rudnicki 2010), and caret (Kuhn 2020) packages.

Results

The classification of the fire-propagating element within the Prometheus system using the MESMA algorithm achieved a very high accuracy (OA = 94.58% and Kappa = 0.92) when assessing all four study sites together (Table 2). The PA and UA for each fire-propagating element showed values consistent with the OA, exceeding 90% in all cases. Therefore, no fire-propagating element was under- or overestimated across the landscape.

Wall-to-wall estimates of the fire-propagating element in the four study sites are shown in Fig. 5. Woodlands dominated the Culebra study site (48% of the surface), particularly in the central strip, while the northern and southern regions presented a much higher landscape spatial heterogeneity. Similarly, woodlands were the predominant landscape feature in the Ladrillar study site (51%), clearly serving as the dominant fire-propagating element in the central and southeastern regions. In contrast, the Bejís and Folgoso study sites displayed a much finer-scale spatial patchiness compared to the previous sites. In Bejís, grasslands (58%) and shrublands (27%) were the dominant fire-propagating elements, whereas in Folgoso, shrublands predominated (46%), followed by woodlands (35%).

In the training dataset corresponding to field plots where shrubs were the dominant fire-propagating element, the Boruta wrapper algorithm around RF identified the following LiDAR-derived metrics as important FT predictors: (i) fuel density in the 0.6–2 m and 2–4 m strata ($D_{0.6–2\ m}$ and $D_{2–4\ m}$), (ii) the vertical complexity index (VCI), and (iii) the leaf area index (LAI). SAR-CR and FCOVER, retrieved from Sentinel-1 and Sentinel-2 data, respectively, were also identified as important predictors (Fig. 6A). In field plots where trees were the dominant fire-propagating element, the Boruta wrapper algorithm also identified LiDAR-derived metrics as the most important predictors. These included (i) fuel density in the 0.3–0.6 m, 0.6–2 m, and 2–4 m strata ($D_{0.3–0.6\ m}$, $D_{0.6–2\ m}$, and $D_{2–4\ m}$), (ii) LAI, (iii) volume of empty voxels (VOX_{EMPTY}), (iv) height of maximum leaf area density (LAD_{MAXH}), (v) depth of the euphotic zone ($EUPH_D$), and (vi) total leaf area in the oligophotic zone ($OLIG_{LA}$). SAR-CR and FCOVER were also consistently selected as relevant predictors (Fig. 6B). Remarkably, most of the variables selected by the Boruta algorithm for the datasets corresponding to each fire-propagating element demonstrated a strong physical and ecological alignment with fuel distribution criteria within the vertical profile used to assign Prometheus FTs. This suggests a high generalization capability of the wall-to-wall FT estimates.

Validations with the independent set of plots in the four study sites showed high accuracy in classifying FTs (OA = 90.27% and Kappa = 0.88; Table 3), confirming the robust generalization capability of the physically based approach proposed in this study. The accuracy for most individual FTs exceeded 80%. The PA and UA of non-fuel areas and the grass FT1 were directly associated with the accuracy of the MESMA-based classification. Shrub FTs were predominantly classified with PA and UA values exceeding 70%. Some confusion was noted between FT2 and FT3, with FT2 exhibiting a UA of 62.50%. This error was caused by the misclassification of three field plots as FT2, which actually correspond to one grass FT1 plot and two FT3 plots. The UA of FT3 was 100%. The accuracy of the FT4 classification was markedly high, with PA and UA equal to 87.50%. Forest FTs were also classified with very high accuracy (PA and UA > 80%). In particular, the PA of FT5 was 100%. A slight overestimation of FT5 was observed due to its assignment to some field plots belonging to FT6.

Wall-to-wall estimates of Prometheus FTs for each study site are shown in Fig. 7. In the Bejís study site, FT1 was the most prevalent class, covering 62% of the area, followed by FTs associated with highly hazardous potential fire behavior, such as FT4 (16%) and FT7 (10%), which were distributed in strips along the northeast-southwest axis. The Culebra study site was equally dominated by FT1 (28%) and FT7 (28%). FT7 exhibited significant spatial continuity across the landscape, primarily along the central axis of the study framework, accompanied by FT5

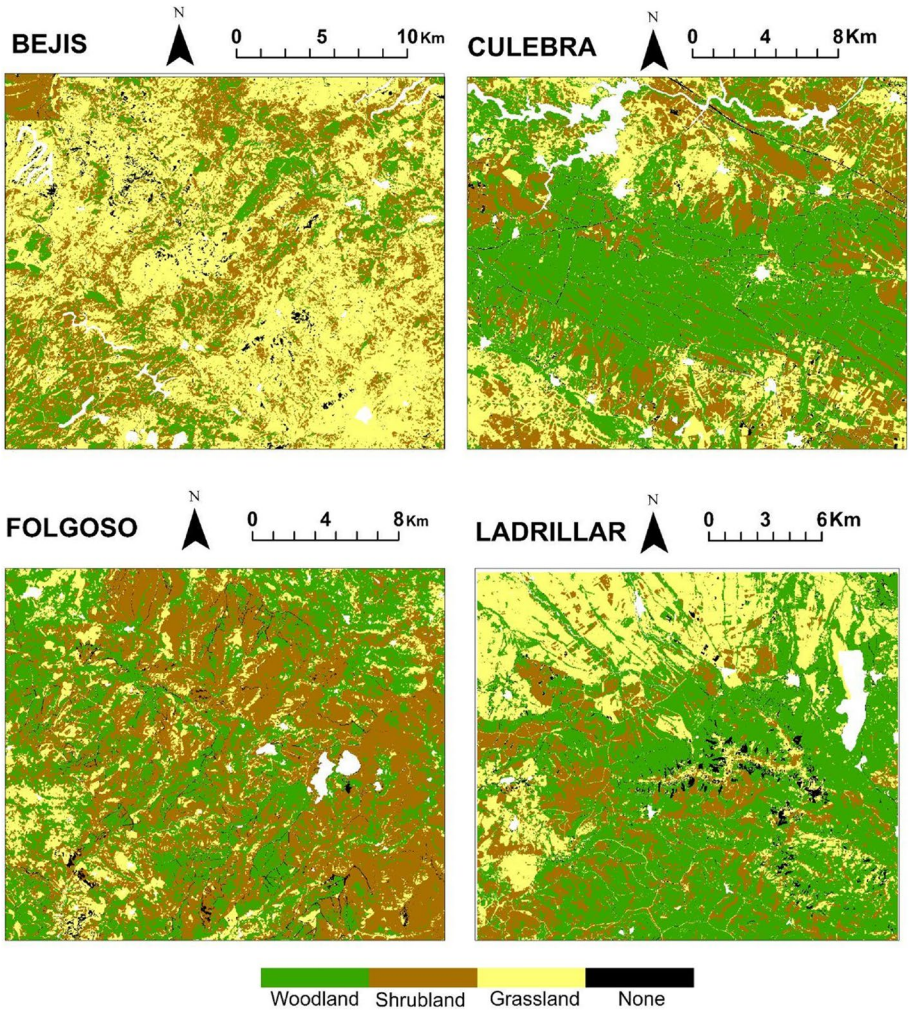

Fig. 5 Wall-to-wall estimates of the fire-propagating element in the Prometheus system across the four study sites. Black pixels labeled "None" indicate locations where no fire-propagating element was assigned by MESMA. White pixels correspond to non-fuel areas masked using layers from the Spanish National Topographic Base

(10%). The distribution of FTs in the Folgoso study site revealed high spatial heterogeneity. FT3 was the most dominant class (30%), particularly along the northwest-southeast axis, followed by FT4 (16%) and FT7 (19%), which were more broadly distributed across the study frame. In the southeastern portion of the Ladrillar study site, forest stands of FT5 (13%) and FT7 (32%) predominated, whereas the northwestern area was characterized by the dominance of FT1 (32%) and FT3 (14%), both displaying notable spatial continuity.

Discussion

The development of accurate fuel type maps is increasingly critical for addressing the growing risks posed by unprecedented extreme wildfire events (Moreira et al. 2020; Abdollahi & Yebra 2023). These maps provide essential information to support preventive measures, fire management strategies, and fire behavior modeling (Aragoneses et al. 2023). In this study, we proposed a novel methodology to characterize both fuel propagation elements and fuel types within the Prometheus system. The methodology was designed for broad applicability by relying exclusively on freely accessible remote sensing data and integrating a comprehensive set of complementary data sources, including multispectral, LiDAR, and SAR, as well as physically based approaches. These elements, along with the accuracy and generalizability demonstrated by validations in four contrasting sites, reveal a significant advancement in this research field. Although the present study focused on classifying discrete fuel types following the Prometheus system, the physically based methods implemented here could be readily extended to predict continuous fuel attributes such as canopy base height, canopy fuel load, or canopy

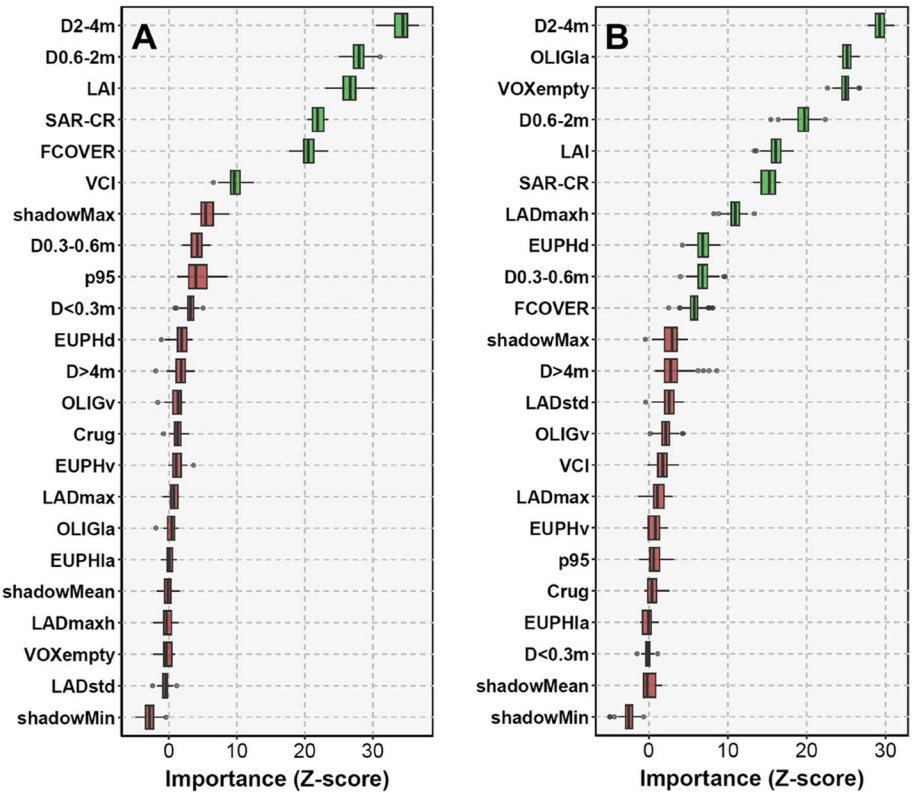

Fig. 6 Variable importance to FT mapping assessed by the Boruta algorithm in training datasets corresponding to field plots where shrubs (**A**) and trees (**B**) were dominant fire-propagating elements. Predictors are sorted by the median of the *Z*-score importance measure. Green boxes correspond to variables deemed to be important by the Boruta algorithm (*Z*-score higher than that of shadowMax internal variable). Variable codes correspond to those shown in Table 1

Table 3 Confusion matrix and accuracy metrics (OA = overall accuracy; PA = producer's accuracy; UA = user's accuracy) for the fuel type (FT) maps using as reference the independent set (30%) of field plots in shrubland ($n = 21$) and woodland ($n = 33$) areas, along with the total number of grassland plots ($n = 34$). An additional set of 25 photointerpreted plots, corresponding to non-fuel areas, were used in the validation process

Prometheus FT		**Reference data**							
		No-fuel	**FT1**	**FT2**	**FT3**	**FT4**	**FT5**	**FT6**	**FT7**
Classified data	**No-fuel**	23	0	0	0	0	0	0	0
	FT1	2	33	1	0	0	0	0	0
	FT2	0	1	5	2	0	0	0	0
	FT3	0	0	0	5	0	0	0	0
	FT4	0	0	0	0	7	0	0	1
	FT5	0	0	0	0	0	12	2	0
	FT6	0	0	0	0	0	0	8	1
	FT7	0	0	0	0	1	0	0	9
	PA (%)	92.00	97.06	83.33	71.43	87.50	100.00	80.00	81.82
	UA (%)	100.00	91.67	62.5	100.00	87.50	85.71	88.89	90.00
	OA (%)	**Kappa**							
	90.27	0.88							

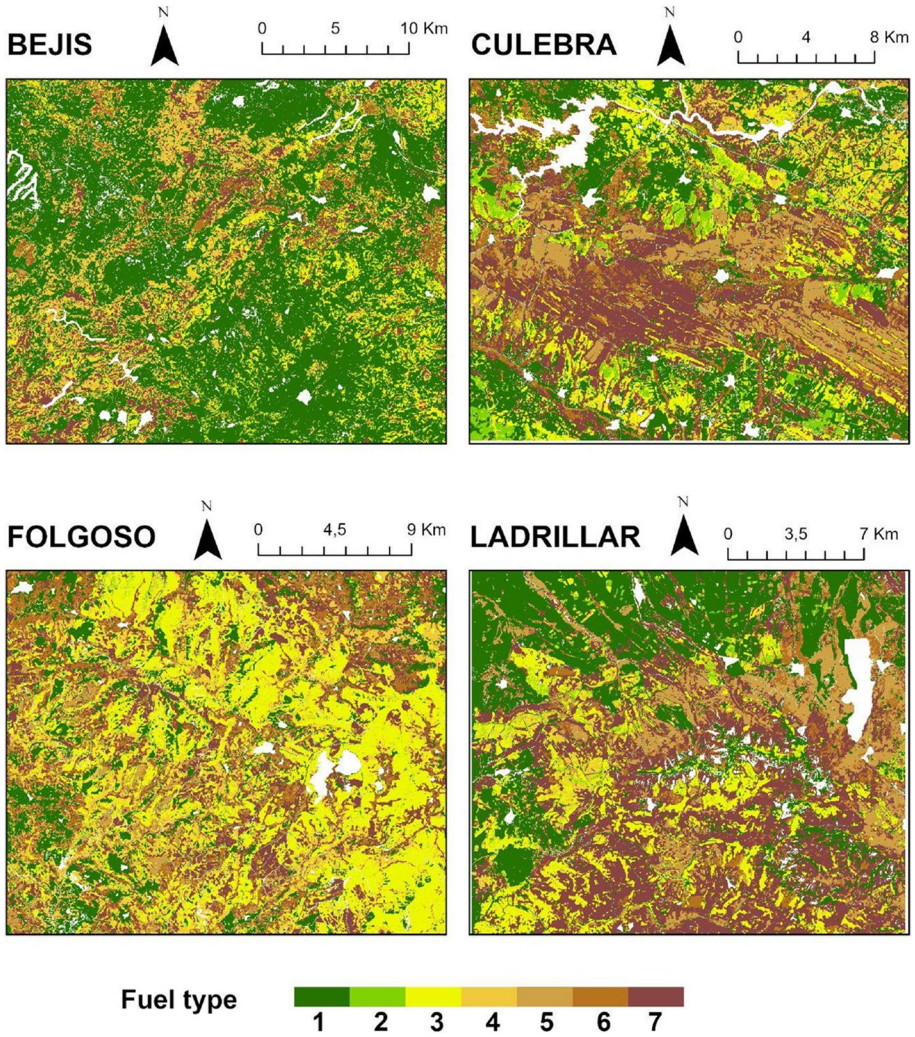

Fig. 7 Wall-to-wall estimates of fuel types (FTs) within the Prometheus system in the four study sites. White pixels correspond to non-fuel areas masked by the Spanish National Topographic Base

bulk density building on previous studies (García et al. 2012; Chamberlain et al. 2021; Aragoneses et al. 2024, 2025). This would provide complementary insights into fuel structure that are critical for enhancing the integration with fire behavior models (Gale et al. 2021).

Our classification of fire propagation elements based on MESMA fraction images and LiDAR metrics has shown to be more accurate (OA = 94.6 and Kappa = 0.9) compared to other classifications methods in previous studies applied to the same (García et al. 2011) or similar (Aragoneses et al. 2023) categories. While previous studies have attained accurate results in single study sites (e.g., OA = 92.8% and Kappa = 0.9 in García et al. 2011), our analysis provides evidence of a high generalization capacity, with a strong performance across four extensive study sites with markedly different plant communities and environmental conditions. The outperformance of the method proposed here can be attributed to the intrinsic characteristics of the applied spectral unmixing technique (MESMA), which provide the fraction of each propagation element within each pixel, in contrast to hard classification methods that fully assign each pixel to a single class or propagation type (e.g., Maximum Likelihood, support vector machine -SVM-, *k*-Nearest Neighbors). This sub-pixel differentiation in fraction images offers several advantages when determining fire propagation elements. First, (i) sub-pixel differentiation is particularly relevant in landscapes with a high spatial heterogeneity, where different propagation elements may coexist at a spatial scale lower than the usual resolution for multispectral satellite images. This is common in mountainous ecosystems, including Mediterranean, Atlantic, and transition zones (Fernández-García et al. 2021), and in European landscapes in general where 27% of

land is composed of patches of < 0.02 km^2 due to human influence over millennia (Antrop 2004). Alternative approaches to deal with these fine-grained landscapes might be the use of very high-resolution data, which are less accessible and computationally costly (García et al. 2011). Second (ii), fraction images allow a subsequent process to align the classification of propagation elements with Prometheus thresholds, which are not fixed to the same value for all classes. For instance, thresholds of cover fraction can be set in 0.6 or 0.5 depending on the target propagation element (e.g., to define FT1 grass, or others, respectively), contrary to hard classifications where classes are invariantly defined according to the predominant class (Fernández-García et al. 2021). Third, the outstanding results of MESMA in differentiating fire propagation elements can be also attributed to its foundation in physically based methods, which differentiate classes departing from an optimal set of spectral signatures. The development of a method grounded in physical basis not only provides logical robustness, but also typically yields more generalizable results, as supported by our accuracy metrics across the four study sites. Nonetheless, the MESMA approach may present several limitations. First, the selected image endmembers for constructing the spectral library must be representative of the spectra of the different classes to be modeled in the scene, as well as spatially generalizable (Quintano et al. 2013), which can pose a significant challenge, especially when high-resolution data for endmember collection are unavailable (Fernández-Guisuraga et al. 2021b). Second, the ability of MESMA to accurately model a large number of land cover classes (e.g., plant communities) remains limited, particularly when accounting for the inherent spectral variability at lower hierarchical levels within the spectral library (Fernández-García et al. 2021; Compains-Iso et al. 2022). These MESMA constraints have not posed a limitation for the Prometheus system, which operates with a limited number of fire-propagating element classes. However, they could present a significant challenge for more detailed fuel classification schemes (e.g., Scott & Burgan 2005; Marino et al. 2016), a topic that warrants further investigation.

After classifying fire propagation data using multispectral imagery and MESMA, a more detailed differentiation of FTs for shrubs and trees was performed to distinguish the seven Prometheus FT categories. In this second stage, both passive and active remote sensing data proved essential, as demonstrated in our analyses, with LiDAR metrics showing the highest importance. Numerous studies have employed a combination of multispectral and LiDAR data (Abdollahi & Yebra 2023), underscoring their complementarity and joint efficacy in accurately mapping FTs, whether within the Prometheus system (e.g., García et al. 2011; Alonso-Benito et al. 2016; Domingo et al. 2020; Hoffrén et al. 2023) or in other classification frameworks (e.g., Mutlu et al. 2008; Marino et al. 2016). Our results indicate a high accuracy in mapping Prometheus FTs (OA = 90.27% and Kappa = 0.88) and, in general, meeting or exceeding the levels reported in previous studies. For example, Domingo et al. (2020) documented an OA of 59% in estimating Prometheus FTs using an SVM algorithm, calibrated with spectral indices from Sentinel-2 and a battery of metrics derived from low-density LiDAR data. Their study covered three areas in eastern Spain, spanning over 200,000 ha. By integrating high-spatial resolution WorldView-2 multispectral imagery with low-density LiDAR data, Alonso-Benito et al. (2016) implemented a geographic object-based image analysis (GEOBIA) methodology to map Prometheus FTs in the Canary Islands, achieving an OA ranging from 76 to 85% in a 15-km^2 study site. Hoffrén et al. (2023) used RF and SVM algorithms to classify Prometheus FTs in a regional-scale study in northeast Spain, excluding FT5 and FT6. Using GEDI L2 A, L2B, and L4 A data combined with Landsat-8 multispectral imagery, they achieved an OA ranging from 82 to 84%. García et al. (2011) achieved an OA of 88% in mapping Prometheus FTs within a 2.7-km^2 region in central Spain. Their approach involved an initial SVM classification using 2-m resolution optical data, followed by a second phase applying decision rules based on LiDAR data with point densities ranging from 1.5 to 6 points m^{-2}. Although similar accuracy was achieved in that study using higher-resolution optical and LiDAR data, the commercial nature and associated costs of these datasets, combined with the relatively small study area, make the generalizability of the results to large-scale FT mapping less evident (Marino et al. 2016). Indeed, greater environmental heterogeneity promotes the existence of a broader spectrum of habitats, which often translates into a wider range of plant communities and differences in their structure (Begon et al. 2006).

The integration of multispectral data with LiDAR metrics is crucial due to LiDAR's capability to characterize the three-dimensional structure of fuels, providing a viable alternative for addressing the main shortcomings associated with mapping FTs solely by means of optical data (Domingo et al. 2020; Abdollahi & Yebra 2023). These tri-dimensional variables are critical for distinguishing FTs in most classification systems, as they often rely on fuel height and fuel continuity criteria (Chuvieco et al. 2003). Specifically, the most important variables in differentiating shrub and tree FTs among the traditional LiDAR metrics were $D_{0.6–2\ m}$ and $D_{2–4\ m}$, which closely resemble understory fuel load and, additionally, ladder fuel density in forest stands (Fernandez-Guisuraga &

Fernandes, 2023) effectively mimicking the Prometheus fuel strata system. In spite of the foregoing, the present study advances the characterization of the three-dimensional structure of fuels and FTs by demonstrating, for the first time, the importance of metrics related to the LAD distribution across vertical fuel layers in FT characterizations. LAD-derived metrics were especially valuable for differentiating tree-dominated FTs (FT5, FT6, and FT7). LAD-related variables may complement traditional LiDAR metrics by capturing more functional characteristics related to forest structure (Detto et al. 2015), including the variability in fuel load distribution across the vertical profile and interactions between fuel layers, such as the vertical connectivity between understory and canopy fuel or the density and continuity of canopy fuel (Kamoske et al. 2019; Viedma et al. 2024; Fernández-Guisuraga, *under review*). For example, the interaction between LAD metrics representing the total leaf area in the oligophotic zone ($OLIG_{LA}$), the height of maximum LAD (LAD_{MAXH}), and the depth of the euphotic zone ($EUPH_{D}$) align well with the Prometheus criteria, which distinguish FT6 and FT7 based on the fuel gap between shrubs and trees. Accurate differentiation of fuel types in treed areas, particularly between FT6 and FT7, is critical, as recent studies suggest that ladder fuels are stronger determinants of burn severity than canopy volumes in Mediterranean forests (Hakkenberg et al. 2024).

The incorporation of SAR cross-polarization ratio (SAR-CR) computed using C-band data, and the FCOVER retrieved from multispectral data, further enhanced the model's performance in predicting shrub and tree FTs. On the one hand, the capacity of SAR-CR to improve FTs mapping may be a consequence of its relationship with vegetation amount and structural complexity across the vertical profile of the plant community, as demonstrated in previous studies (Fernández-García et al. 2023; Fernández-Guisuraga et al. 2024). On the other hand, the FCOVER as a biophysical variable adds value by distinguishing patterns in the ratio of photosynthetic and non-photosynthetic material within the community (Fernández-Guisuraga et al. 2021a) either at the top-of-canopy in shrub and tree FTs, or through canopy gaps in tree-dominated FTs. We suspect that the synergy between LiDAR and SAR data in characterizing the vertical profile of the plots, along with the incorporation of a vegetation biophysical variable, likely contributed to the reduced confusion between FT7 and FT5 compared to previous studies that relied solely on higher-density LiDAR data in the second phase of the FT estimation (e.g., García et al. 2011). Nonetheless, this synergy may not have been sufficient to adequately sample through a dense forest canopy the lower fuel load in the understory of FT6 plots compared to FT7 due to the low density of the LiDAR point clouds (Marino et al. 2016) and the signal attenuation of C-band SAR, hence the misclassification of several FT6 plots as FT5. In connection with the above, the confusion evidenced in the classification of shrub FTs, particularly between FT2 and FT3, may be partly explained by the well-documented underestimation of shrub height when using low-density LiDAR data (Mitchell et al. 2011; Li et al. 2015; Fernández-Guisuraga et al. 2022b), and by the similar roughness of low shrub canopies as to cause a differential SAR backscatter behavior (ESA 2007; Meyer 2019; Fernández-Guisuraga et al. 2023a, b).

Despite the high accuracy in the estimation of FTs within the Prometheus system in this study, there is still room for improvement by leveraging cutting-edge remote sensing data. For example, very high-density LiDAR data acquired from sensors onboard unmanned aerial vehicles (UAVs) have been shown in previous studies to characterize very accurately the fine-scale community structure in forest stands (Hyyppä et al. 2020) and shrublands (Sankey et al. 2018; Fernández-Guisuraga et al., 2024b). While this approach may have limited spatial coverage for mapping FTs at broader spatial scales, combining UAV-LiDAR data with airborne LiDAR and multispectral data through hierarchical model-based inference has been demonstrated to provide more accurate estimates than methods relying on a single data source (Puliti et al. 2018; Saarela et al. 2018). Similarly, the use of L- and P-band SAR data may enhance the prediction of FTs due to their greater canopy penetration compared to shorter wavelengths (i.e., C-band) (Tanase et al. 2014). Indeed, Saatchi et al. (2007) found that P-band data provided highly accurate estimates of individual fuel parameters in mature forests, whereas L-band data proved more effective for estimating fuel parameters in shrublands and young forests.

Conclusions

The development of accurate FT maps is crucial to address the increasing risks posed by extreme wildfire events, providing essential information for management strategies and fire behavior modeling. This study introduces a novel methodology for FT characterization within the Prometheus system, leveraging freely available remote sensing data sources, including multispectral, LiDAR, and SAR datasets, supported by physically based approaches. The proposed methodology demonstrated high accuracy and generalizability across four extensive and contrasting study sites, reflecting its potential for broad-scale applications. Our findings highlight the effectiveness of MESMA in accurately mapping fire propagation elements, with sub-pixel differentiation offering significant advantages over traditional

hard-classification methods. This was particularly relevant in heterogeneous landscapes, where the coexistence of propagation elements occurs at scales below the resolution of standard multispectral satellite imagery. Furthermore, the integration of multispectral and active remote sensing data proved critical for the detailed differentiation of Prometheus FTs, achieving a high accuracy and surpassing the performance of previous studies in generalization capacity. LiDAR metrics were identified as the most influential variables for differentiating shrub and tree FTs, particularly those related to understory and ladder fuels. Importantly, this study advances the field by demonstrating, for the first time, the relevance of LAD-derived metrics in FT characterization, providing a more functional and detailed understanding of the vertical fuel structure. These metrics effectively capture vertical connectivity and the spatial variability of fuel loads, aligning well with the Prometheus system's criteria and addressing key limitations of traditional LiDAR metrics. Additionally, the inclusion of SAR-CR and biophysical variables such as FCOVER enhanced the classification performance, with SAR-CR reflecting vertical structural complexity and FCOVER distinguishing photosynthetic and non-photosynthetic material across vegetation types. However, some challenges remain, including the misclassification of certain FTs due to the limitations of low-density LiDAR data and C-band SAR signal attenuation.

Abbreviations

CHM	Canopy height model
CRUG	Canopy rugosity
CSF	Cloth simulation filter
DTM	Digital terrain model
EUPHD	Depth of the euphotic zone
EUPHLA	Total leaf area in the euphotic zone
EUPHV	Volume of the euphotic zone
FBP	Canadian Forest Fire Behavior Prediction
FCOVER	Fractional vegetation cover
FT	Fuel type
GEE	Google Earth Engine
GEOBIA	Geographic object-based image analysis
GRD	Ground range detected
IES	Iterative Endmember Selection
LAD	Leaf area density
LADMAX	Maximum LAD
LADMAXH	Height of maximum LAD
LADSTD	Standard deviation of LAD
LAI	Leaf area index
LiDAR	Light detection and ranging
MCC	Multiscale curvature classification
MESMA	Multiple endmember spectral mixture analysis
NFFL	Northern Forest Fire Laboratory
OA	Overall accuracy
OLIGLA	Total leaf area in the oligophotic zone
OLIGV	Volume of the oligophotic zone
PA	Producer's accuracy
PMF	Progressive morphological filter
PNOA	Spanish National Plan for Aerial Orthophotography
RF	Random Forest
RMSE	Root mean square error
RTM	Radiative transfer model
SAR	Synthetic aperture radar
SAR-CR	SAR cross-polarization ratio
SFM25	Spanish Forest Map at 1:25,000
SMA	Spectral mixture analysis
SVM	Support vector machine
TIN	Triangulated irregular network
UA	User's accuracy
VCI	Vertical complexity index
VIPER	Visualization and Image Processing for Environmental Research
VOXEMPTY	Volume of empty voxels

Authors' contributions

JMF-G: Conceptualization, Methodology, Investigation, Formal analysis, Writing—original draft, Supervision. AM: Investigation, Methodology, Writing—original draft. VF-G: Conceptualization, Writing—original draft. SAPP: Methodology, Formal analysis. LC: Conceptualization, Investigation, Writing—review & editing, Supervision, Funding acquisition.

Funding

This study was financially supported by the Spanish Ministry of Science and Innovation in the framework of LANDSUSFIRE project (PID2022-139156OB-C21) within the National Program for the Promotion of Scientific-Technical Research (2021–2023), by the Regional Government of Castile and León in the framework of the IA-FIREXTCyL project (LE081P23) and by the Fundación Biodiversidad of the Ministry for the Ecological Transition and the Demographic Challenge (MITECO) within the framework of the Recovery, Transformation, and Resilience Plan (PRTR), funded by the European Union – NextGenerationEU in the framework of the "Sistemas agroforestales multifuncionales como alternativa a la conservación del paisaje: AGROFORES" BF 273. Andrea Monzón-Gonzalez was supported by pre-doctoral fellowship from the University of León.

Data availability

The datasets generated and used during the current study are available from the corresponding author on reasonable request.

Declarations

Ethics approval and consent to participate

Not applicable.

Consent for publication

Not applicable.

Competing interests

The authors declare that they have no competing interests.

Author details

[1]Department of Biodiversity and Environmental Management, Faculty of Biological and Environmental Sciences, University of León, León 24071, Spain. [2]Institute of Environmental Research, Natural Resources and Biodiversity (IMARENABIO), University of León, León 24071, Spain. [3]Centre for the Research and Technology of Agro-Environment and Biological Sciences (CITAB), University of Trás-Os-Montes and Alto Douro, Vila Real 5000-801, Portugal. [4]Institute of Geography and Sustainability, Faculty of Geosciences and Environment, Université de Lausanne, Geópolis, Lausanne CH-1015, Switzerland. [5]Department of Geography and Geology, Faculty of Philosophy and Letters, University of León, León 24071, Spain. [6]Centre of Excellence for Safety Research (CESAR), Faculty of Safety Engineering, Technical University of Ostrava, Ostrava-Poruba 708 00, Czech Republic.

Received: 29 January 2025 Accepted: 8 April 2025
Published online: 12 May 2025

References

Abdollahi, A., and M. Yebra. 2023. Forest fuel type classification: Review of remote sensing techniques, constraints and future trends. *Journal of Environmental Management* 342: 118315. https://doi.org/10.1016/j.jenvman.2023.118315.

Alberdi, I., V. Sandoval, S. Condés, I. Cañellas, and R. Vallejo. 2016. El Inventario Forestal Nacional español, una herramienta para el conocimiento, la gestión y la conservación de los ecosistemas forestales arbolados. *Ecosistemas: Revista Cietifica y Tecnica De Ecologia y Medio Ambiente* 25 (3): 88–97. https://doi.org/10.7818/ecos.2016.25-3.10.

Albini, F. A. 1976. Estimating wildfire behavior and effects. Gen. Tech. Rep. INT-GTR-30. U.S. Department of Agriculture, Forest Service, *Intermountain Forest and Range Experiment Station*.

Alonso-Benito, A., L.A. Arroyo, M. Arbelo, and P. Hernández-Leal. 2016. Fusion of WorldView-2 and LiDAR Data to Map Fuel Types in the Canary Islands. *Remote Sensing* 8 (8): 669. https://doi.org/10.3390/rs8080669.

Anderson, HE. 1982. Aids to determining fuel models for estimating fire behavior. Gen. Tech. Rep. INT-GTR-122, 22. Ogden: U.S.Department of Agriculture, Forest Service, Intermountain Forest and Range Experiment Station.

Antrop, M. 2004. Landscape change and the urbanization process in Europe. *Landscape and Urban Planning* 67 (1–4): 9–26. https://doi.org/10.1016/S0169-2046(03)00026-4.

Aragoneses, E., and E. Chuvieco. 2021. Generation and Mapping of Fuel Types for Fire Risk Assessment. *Fire* 4 (3). https://doi.org/10.3390/fire4030059.

Aragoneses, E., M. García, M. Salis, L.M. Ribeiro, and E. Chuvieco. 2023. Classification and mapping of European fuels using a hierarchical, multipurpose fuel classification system. *Earth System Science Data* 15 (3): 1287–1315. https://doi.org/10.5194/essd-15-1287-2023.

Aragoneses, E., M. García, P. Ruiz-Benito, and E. Chuvieco. 2024. Mapping forest canopy fuel parameters at European scale using spaceborne LiDAR and satellite data. *Remote Sensing of Environment* 303: 114005. https://doi.org/10.1016/j.rse.2024.114005.

Aragoneses, E., M. García, H. Tang, and E. Chuvieco. 2025. A multi-sensor approach allows confident mapping of forest canopy fuel load and canopy bulk density to assess wildfire risk at the European scale. *Remote Sensing of Environment* 318: 114578. https://doi.org/10.1016/j.rse.2024.114578.

Arroyo, L.A., S.P. Healey, W.B.D. Cohen, D. Cocero, and J.A. Manzanera. 2006. Using object-oriented classification and high-resolution imagery to map fuel types in a Mediterranean region. *Journal of Geophysical Research* 111: G04S04. https://doi.org/10.1029/2005jg000120.

Axelsson, P. 2000. DEM generation from laser scanner data using adaptive TIN models. *International Archives of Photogrammetry and Remote Sensing* 33 (4): 110–117.

Begon, M., C.R. Townsend, and J.L. Harper. 2006. *Ecology: From Individuals to Ecosystems*. New York: Wiley.

Belenguer-Plomer, M.A., M.A. Tanase, A. Fernandez-Carrillo, and E. Chuvieco. 2019. Burned area detection and mapping using Sentinel-1 backscatter coefficient and thermal anomalies. *Remote Sensing of Environment* 233: 111345. https://doi.org/10.1016/j.rse.2019.111345.

Benali, A., A.C.L. Sá, A.R. Ervilha, R.M. Trigo, P.M. Fernandes, and J.M.C. Pereira. 2017. Fire spread predictions: Sweeping uncertainty under the rug. *Science of the Total Environment* 592: 187–196. https://doi.org/10.1016/j.scitotenv.2017.03.106.

Breiman, L. 2001. Random forests. *Machine Learning* 45 (1): 5–32. https://doi.org/10.1023/a:1010933404324.

Cardil, A., S. Monedero, G. Schag, and S. de-Miguel, M. Tapia, C.R. Stoof, C.A. Silva, M. Mohan, A. Cardil, and J. Ramirez. 2021. Fire behavior modeling for operational decision-making. *Current Opinion in Environmental Science & Health* 23: 100291. https://doi.org/10.1016/j.coesh.2021.100291.

Chamberlain, C.P., A.J. Sánchez Meador, and A.E. Thode. 2021. Airborne lidar provides reliable estimates of canopy base height and canopy bulk density in southwestern ponderosa pine forests. *Forest Ecology and Management* 481: 118695. https://doi.org/10.1016/j.foreco.2020.118695.

Chuvieco, E., D. Riaño, J. Van Wagtendok, and F. Morsdof. 2003. Fuel loads and fuel type mapping. *Wildland fire danger estimation and mapping* 119–142. https://doi.org/10.1142/9789812791177_0005.

European Commission. 1999. *Prometheus: Management techniques for optimization of suppression and minimization of wildfire effects.* System Validation. Nos. ENV4-CT98–0716. European Commission.

Compains-Iso, L., A. Fernández-Manso, and V. Fernández-García. 2022. Optimizing Spectral Libraries from Landsat Imagery for the Analysis of Habitat Richness Using MESMA. *Forests* 13 (11): 1824. https://doi.org/10.3390/f13111824.

Dennison, P.E., and D.A. Roberts. 2003. Endmember selection for multiple endmember spectral mixture analysis using endmember average RMSE. *Remote Sensing of Environment* 87 (2–3): 123–135. https://doi.org/10.1016/S0034-4257(03)00135-4.

Detto, M., G.P. Asner, H.C. Muller-Landau, and O. Sonnentag. 2015. Spatial variability in tropical forest leaf area density from multireturn lidar and modeling: Multireturn LiDAR and tropical forest. *Journal of Geophysical Research: Biogeosciences* 120: 294–309. https://doi.org/10.1002/2014JG002774.

Domingo, D., J. de la Riva, M.T. Lamelas, A. García-Martín, P. Ibarra, M. Echeverría, and R. Hoffrén. 2020. Fuel Type Classification Using Airborne Laser Scanning and Sentinel 2 Data in Mediterranean Forest Affected by Wildfires. *Remote Sensing* 12 (21): 3660. https://doi.org/10.3390/rs12213660.

Engelstad, P.S., M. Falkowski, P. Wolter, A. Poznanovic, and P. Johnson. 2019. Estimating canopy fuel attributes from low-Density LiDAR. *Fire* 2 (3): 38. https://doi.org/10.3390/fire2030038.

ESA. 2007. ASAR Product Handbook. Issue 2.2. https://earth.esa.int/eogateway/documents/20142/37627/ASAR-Product-Handbook.pdf.

Evans, J.S., and A.T. Hudak. 2007. A multiscale curvature algorithm for classifying discrete return LiDAR in forested environments. *IEEE Transactions on Geoscience and Remote Sensing* 45 (4): 1029–1038. https://doi.org/10.1109/tgrs.2006.890412.

Feilhauer, H., and S. Schmidtlein. 2011. On variable relations between vegetation patterns and canopy reflectance. *Ecological Informatics* 6 (2): 83–92. https://doi.org/10.1016/j.ecoinf.2010.12.004.

Fernández-García, V., E. Marcos, J.M. Fernández-Guisuraga, A. Fernández-Manso, C. Quintano, S. Suárez-Seoane, and L. Calvo. 2021. Multiple Endmember Spectral Mixture Analysis (MESMA) Applied to the Study of Habitat Diversity in the Fine-Grained Landscapes of the Cantabrian Mountains. *Remote Sensing* 13 (5): 979. https://doi.org/10.3390/rs13050979.

Fernández-García, V., D. Beltrán-Marcos, J.M. Fernández-Guisuraga, E. Marcos, and L. Calvo. 2022. Predicting potential wildfire severity across Southern Europe with global data sources. *Science of the Total Environment* 829: 154729. https://doi.org/10.1016/j.scitotenv.2022.154729.

Fernández-García, V., D. Beltrán-Marcos, and L. Calvo. 2023. Building patterns and fuel features drive wildfire severity in wildland-urban interfaces in Southern Europe. *Landscape and Urban Planning* 231: 104646. https://doi.org/10.1016/j.landurbplan.2022.104646.

Fernández-Guisuraga, J.M., and P.M. Fernandes. 2023. Using Pre-Fire High Point Cloud Density LiDAR Data to Predict Fire Severity in Central Portugal. *Remote Sensing* 15 (3): 768. https://doi.org/10.3390/rs15030768.

Fernández-Guisuraga, J.M., and P.M. Fernandes. 2024. Enhanced post-wildfire vegetation recovery in prescribed-burnt Mediterranean shrubland: A regional assessment. *Forest Ecology and Management* 561: 121921. https://doi.org/10.1016/j.foreco.2024.121921.

Fernández-Guisuraga, J.M., L. Calvo, and S. Suárez-Seoane. 2020. Comparison of pixel unmixing models in the evaluation of post-fire forest resilience based on temporal series of satellite imagery at moderate and very high spatial resolution. *ISPRS Journal of Photogrammetry and Remote Sensing* 164: 217–228. https://doi.org/10.1016/j.isprsjprs.2020.05.004.

Fernández-Guisuraga, J.M., S. Suárez-Seoane, and L. Calvo. 2021a. Radiative transfer modeling to measure fire impact and forest engineering resilience at short-term. *ISPRS Journal of Photogrammetry and Remote Sensing* 176: 30–41. https://doi.org/10.1016/j.isprsjprs.2021.04.002.

Fernández-Guisuraga, J.M., J. Verrelst, L. Calvo, and S. Suárez-Seoane. 2021b. Hybrid inversion of radiative transfer models based on high spatial resolution satellite reflectance data improves fractional vegetation cover retrieval in heterogeneous ecological systems after fire. *Remote Sensing of Environment* 255: 112304. https://doi.org/10.1016/j.rse.2021.112304.

Fernández-Guisuraga, J.M., S. Suárez-Seoane, P.M. Fernandes, V. Fernández-García, A. Fernández-Manso, C. Quintano, and L. Calvo. 2022a. Pre-fire aboveground biomass, estimated from LiDAR, spectral and field inventory data, as a major driver of burn severity in maritime pine (*Pinus pinaster*) ecosystems. *Forest Ecosystems* 9: 100022. https://doi.org/10.1016/j.fecs.2022.100022.

Fernández-Guisuraga, J.M., L. Calvo, P.M. Fernandes, and S. Suárez-Seoane. 2022b. Short-Term Recovery of the Aboveground Carbon Stock in Iberian Shrublands at the Extremes of an Environmental Gradient and

as a Function of Burn Severity. *Forests* 13 (2): 145. https://doi.org/10.3390/f13020145.

Fernández-Guisuraga, J.M., S. Súarez-Seoane, and L. Calvo. 2023a. Radar and multispectral remote sensing data accurately estimate vegetation vertical structure diversity as a fire resilience indicator. *Remote Sensing in Ecology and Conservation* 9 (1): 117–132. https://doi.org/10.1002/rse2.299.

Fernández-Guisuraga, J.M., L. Calvo, C. Quintano, A. Fernández-Manso, and P.M. Fernandes. 2023b. Fractional vegetation cover ratio estimated from radiative transfer modeling outperforms spectral indices to assess fire severity in several Mediterranean plant communities. *Remote Sensing of Environment* 290: 113542. https://doi.org/10.1016/j.rse.2023.113542.

Fernández-Guisuraga, J.M., I. González-Pérez, A. Reguero-Vaquero, and E. Marcos. 2024a. Estimating Grassland Biophysical Parameters in the Cantabrian Mountains Using Radiative Transfer Models in Combination with Multiple Endmember Spectral Mixture Analysis. *Remote Sensing* 16 (23): 4547. https://doi.org/10.3390/rs16234547.

Fernández-Guisuraga, J.M., L. Calvo, J. Enterkine, W.J. Price, J.B. Dinkins, K.S. Jensen, P.J. Olsoy, and S.A. Arispe. 2024b. Estimating vegetation and litter biomass fractions in rangelands using structure-from-motion and LiDAR datasets from unmanned aerial vehicles. *Landscape Ecology* 39 (10): 1–19. https://doi.org/10.1007/s10980-024-01979-w.

Gale, M.G., G.J. Cary, A.I.J.M. Van Dijk, and M. Yebra. 2021. Forest fire fuel through the lens of remote sensing: Review of approaches, challenges and future directions in the remote sensing of biotic determinants of fire behaviour. *Remote Sensing of Environment* 255: 112282. https://doi.org/10.1016/j.rse.2020.112282.

García, M., D. Riaño, E. Chuvieco, J. Salas, and F.M. Danson. 2011. Multispectral and LiDAR data fusion for fuel type mapping using Support Vector Machine and decision rules. *Remote Sensing of Environment* 115 (6): 1369–1379. https://doi.org/10.1016/j.rse.2011.01.017.

García, M., S. Popescu, D. Riaño, K. Zhao, A. Neuenschwander, M. Agca, and E. Chuvieco. 2012. Characterization of canopy fuels using ICESat/GLAS data. *Remote Sensing of Environment* 123: 81–89. https://doi.org/10.1016/j.rse.2012.03.018.

Hakkenberg, C.R., M.L. Clark, T. Bailey, P. Burns, and S.J. Goetz. 2024. Ladder fuels rather than canopy volumes consistently predict wildfire severity even in extreme topographic-weather conditions. *Communications Earth & Environment* 5 (1): 1–11. https://doi.org/10.1038/s43247-024-01893-8.

Hardiman, B.S., G. Bohrer, C.M. Gough, C.S. Vogel, and P.S. Curtis. 2011. The role of canopy structural complexity in wood net primary production of a maturing northern deciduous forest. *Ecology* 92 (9): 1818–1827. https://doi.org/10.1890/10-2192.1.

Hillman, S., B. Hally, L. Wallace, D. Turner, A. Lucieer, K. Reinke, and S. Jones. 2021. High-Resolution Estimates of Fire Severity—An Evaluation of UAS Image and LiDAR Mapping Approaches on a Sedgeland Forest Boundary in Tasmania. *Australia. Fire* 4 (1): 14. https://doi.org/10.3390/fire4010014.

Hoffrén, R., M.T. Lamelas, J. de la Riva, D. Domingo, A.L. Montealegre, A. García-Martín, and S. Revilla. 2023. Assessing GEDI-NASA system for forest fuels classification using machine learning techniques. *International Journal of Applied Earth Observation and Geoinformation* 116: 103175. https://doi.org/10.1016/j.jag.2022.103175.

Hoffrén, R., M.T. Lamelas, and J. de la Riva. 2024. Classification and Mapping of Fuels in Mediterranean Forest Landscapes Using a UAV-LiDAR System and Integration Possibilities with Handheld Mobile Laser Scanner Systems. *Remote Sensing* 16 (18): 3536. https://doi.org/10.3390/rs16183536.

Hościło, A., and A. Lewandowska. 2019. Mapping Forest Type and Tree Species on a Regional Scale Using Multi-Temporal Sentinel-2 Data. *Remote Sensing* 11 (8): 929. https://doi.org/10.3390/rs11080929.

Huesca, M., D. Riaño, and S.L. Ustin. 2019. Spectral mapping methods applied to LiDAR data: Application to fuel type mapping. *International Journal of Applied Earth Observation and Geoinformation* 74: 159–168. https://doi.org/10.1016/j.jag.2018.08.020.

Hummel, S., A.T. Hudak, E.H. Uebler, M.J. Falkowski, and K.A. Megown. 2011. A Comparison of Accuracy and Cost of LiDAR versus Stand Exam Data for Landscape Management on the Malheur National Forest. *Journal of Forestry* 109 (5): 267–273. https://doi.org/10.1093/jof/109.5.267.

Hyyppä, E., J. Hyyppä, T. Hakala, A. Kukko, M.A. Wulder, J.C. White, J. Pyörälä, X. Yu, Y. Wang, J.-P. Virtanen, O. Pohjavirta, X. Liang, M. Holopainen, and H. Kaartinen. 2020. Under-Canopy UAV Laser Scanning for Accurate Forest Field Measurements. *ISPRS Journal of Photogrammetry and Remote Sensing* 164: 41–60. https://doi.org/10.1016/j.isprsjprs.2020.03.021.

Jakubowksi, M.K., Q. Guo, B. Collins, S. Stephens, and M. Kelly. 2013. Predicting Surface Fuel Models and Fuel Metrics Using Lidar and CIR Imagery in a Dense, Mountainous Forest. *Photogrammetric Engineering and Remote Sensing* 79 (1): 37–49. https://doi.org/10.14358/pers.79.1.37.

Kamoske, A.G., K.M. Dahlin, S.C. Stark, and S.P. Serbin. 2019. Leaf area density from airborne LiDAR: Comparing sensors and resolutions in a temperate broadleaf forest ecosystem. *Forest Ecology and Management* 433: 364–375. https://doi.org/10.1016/j.foreco.2018.11.017.

Kamoske, A.G., K.M. Dahlin, Q.D. Read, S. Record, S.C. Stark, S.P. Serbin, and P.L. Zarnetske. 2022. Towards mapping biodiversity from above: Can fusing lidar and hyperspectral remote sensing predict taxonomic, functional, and phylogenetic tree diversity in temperate forests? *Global Ecology and Biogeography* 31 (7): 1440–1460. https://doi.org/10.1111/geb.13516.

Keeley, J.E., W.J. Bond, R.A. Bradstock, J.G. Pausas, and P.W. Rundel. 2011. Fire in mediterranean ecosystems: Ecology, evolution and management. *Cambridge University Press*. https://doi.org/10.1017/cbo9781139033091.

Kuhn, M. 2020. *Caret: Classification and Regression Training*. R package version 6.0–86. Available from: https://cran.r-project.org/package=caret.

Kursa, M.B., and W.R. Rudnicki. 2010. Feature Selection with the Boruta Package. *Journal of Statistical Software* 36 (11): 1–13. https://doi.org/10.18637/jss.v036.i11.

Kwak, D.A., G. Cui, W.K. Lee, H.K. Cho, S.W. Jeon, and S.H. Lee. 2014. Estimating plot volume using lidar height and intensity distributional parameters. *International Journal of Remote Sensing* 35 (13): 4601–4629. https://doi.org/10.1080/01431161.2014.915592.

Lefsky, M.A., W.B. Cohen, S.A. Acker, G.G. Parker, T.A. Spies, and D. Harding. 1999. Lidar Remote Sensing of the Canopy Structure and Biophysical Properties of Douglas-Fir Western Hemlock Forests. *Remote Sensing of Environment* 70 (3): 339–361. https://doi.org/10.1016/s0034-4257(99)00052-8.

Li, A., N.F. Glenn, P.J. Olsoy, J.J. Mitchell, and R. Shrestha. 2015. Aboveground Biomass Estimates of Sagebrush Using Terrestrial and Airborne LiDAR Data in a Dryland Ecosystem. *Agricultural and Forest Meteorology* 213: 138–147. https://doi.org/10.1016/j.agrformet.2015.06.005.

Liaw, A., and M. Wiener. 2002. Classification and regression by randomForest. *R News* 2 (3): 18–22. https://cran.r-project.org/doc/Rnews/.

Mallinis, G., G. Galidaki, and I.A. Gitas. 2014. Comparative Analysis of EO-1 Hyperion, Quickbird and Landsat TM Imagery for Fuel Type Mapping of a Typical Mediterranean Landscape. *Remote Sensing* 6: 1684–1704. https://doi.org/10.3390/rs6021684.

Marino, E., P. Ranz, J.L. Tomé, M.Á. Noriega, J. Esteban, and J. Madrigal. 2016. Generation of high-resolution fuel model maps from discrete airborne laser scanner and Landsat-8 OLI: A low-cost and highly updated methodology for large areas. *Remote Sensing of Environment* 187: 267–280. https://doi.org/10.1016/j.rse.2016.10.020.

Martin-Ducup, O., J.L. Dupuy, M. Soma, J. Guerra-Hernandez, E. Marino, P.M. Fernandes, A. Just, J. Corbera, M. Toutchkov, C. Sorribas, J. Bock, A. Piboule, F. Pirotti, and F. Pimont. 2025. Unlocking the potential of Airborne LiDAR for direct assessment of fuel bulk density and load distributions for wildfire hazard mapping. *Agricultural and Forest Meteorology* 362: 110341. https://doi.org/10.1016/j.agrformet.2024.110341.

Meyer, F. 2019. Spaceborne synthetic aperture radar – principles, data access, and basic processing techniques. In *SAR handbook: Comprehensive methodologies for forest monitoring and biomass estimation*, edited by A. Flores, K. Herndon, R. Thapa, & E. Cherrington, 21–64. NASA.

Mitchell, J. J., N. F. Glenn, T. T. Sankey, D. R. Derryberry, M. O. Anderson, and R. C. Hruska. 2011. Small-footprint Lidar Estimations of Sagebrush Canopy Characteristics. *Photogrammetric Engineering & Remote Sensing* 77 (5): 521–530. https://doi.org/10.14358/PERS.77.5.521.

Moran, C.J., E.M. Rowell, and C.A. Seielstad. 2018. A data-driven framework to identify and compare forest structure classes using LiDAR. *Remote Sensing of Environment* 211: 154–166. https://doi.org/10.1016/j.rse.2018.04.005.

Moreira, F., O. Viedma, M. Arianoutsou, T. Curt, N. Koutsias, E. Rigolot, A. Barbati, P. Corona, P. Vaz, G. Xanthopoulos, F. Mouillot, and E. Bilgili. 2011. Landscape – wildfire interactions in southern Europe: Implications for landscape management. *Journal of Environmental Management* 92 (10): 2389–2402. https://doi.org/10.1016/j.jenvman.2011.06.028.

Moreira, F., D. Ascoli, H. Safford, M. A. Adams, J. M. Moreno, J. M. C. Pereira, F. X. Catry, J. Armesto, W. Bond, and M. E. González. 2020. Wildfire management in Mediterranean-type regions: paradigm change needed.

Environmental Research Letters 15 (1). https://doi.org/10.1088/1748-9326/ab541e.

Moritz, M.A., M.A. Parisien, E. Batllori, M.A. Krawchuk, J. Van Dorn, D.J. Ganz, K. Hayhoe, M.A. Moritz, M.A. Parisien, E. Batllori, M.A. Krawchuk, J. Van, D.J. Dorn, and Ganz, and K. Hayhoe. 2012. Climate change and disruptions to global fire activity. *Ecosphere* 3 (6): 1–22. https://doi.org/10.1890/es11-00345.1.

Moritz, M.A., E. Batllori, R.A. Bradstock, A.M. Gill, J. Handmer, P.F. Hessburg, J. Leonard, S. McCaffrey, D.C. Odion, T. Schoennagel, and A.D. Syphard. 2014. Learning to coexist with wildfire. *Nature* 515 (7525): 58–66. https://doi.org/10.1038/nature13946.

Morsdorf, F., B. Kötz, E. Meier, K.I. Itten, and B. Allgöwer. 2006. Estimation of LAI and fractional cover from small footprint airborne laser scanning data based on gap fraction. *Remote Sensing of Environment* 104 (1): 50–61. https://doi.org/10.1016/j.rse.2006.04.019.

Mutlu, M., S.C. Popescu, C. Stripling, and T. Spencer. 2008. Mapping surface fuel models using lidar and multispectral data fusion for fire behavior. *Remote Sensing of Environment* 112 (1): 274–285. https://doi.org/10.1016/j.rse.2007.05.005.

Næsset, E., O.M. Bollandsås, and T. Gobakken. 2005. Comparing regression methods in estimation of biophysical properties of forest stands from two different inventories using laser scanner data. Remote Sensing of Environment 94:541–553.

Ninyerola, M., X. Pons, and J.M. Roure. 2005. *Atlas Climático Digital de la Península Ibérica*. Centre de Recerca Ecológica i Aplicacions Forestals: Metodología y aplicaciones en bioclimatología y geobotánica. Universidad autónoma de Barcelona.

Oswald, B.P., J.T. Fancher, D.L. Kulhavy, and H.C. Reeves. 1999. Classifying fuels with aerial photography in East Texas. *International Journal of Wildland Fire* 9 (2): 109–113. https://doi.org/10.1071/WF00002.

Patenaude, G., R. Milne, and T.P. Dawson. 2005. Synthesis of Remote Sensing Approaches for Forest Carbon Estimation: Reporting to the Kyoto Protocol. *Environmental Science & Policy* 8: 161–178. https://doi.org/10.1016/j.envsci.2004.12.010.

Pausas, J.G., and J.E. Keeley. 2021. Wildfires and global change. *Frontiers in Ecology and the Environment* 19 (7): 387–395. https://doi.org/10.1002/fee.2359.

Picotte, J.J., and K.M. Robertson. 2011. Validation of remote sensing of burn severity in south-eastern US ecosystems. *International Journal of Wildland Fire* 20 (3): 453–464. https://doi.org/10.1071/wf10013.

Probst, P., and A.L. Boulesteix. 2018. To Tune or Not to Tune the Number of Trees in Random Forest. *Journal of Machine Learning Research* 18 (181): 1–18. https://doi.org/10.48550/arXiv.1705.05654.

Puliti, S., S. Saarela, T. Gobakken, G. Ståhl, and E. Næsset. 2018. Combining UAV and Sentinel-2 Auxiliary Data for Forest Growing Stock Volume Estimation Through Hierarchical Model-Based Inference. *Remote Sensing of Environment* 204: 485–497. https://doi.org/10.1016/j.rse.2017.10.007.

Pyne, Stephen J., Philip L. Andrews, and Richard D. Laven. 1996. *Introduction to Wildland Fire*. New York: John Wiley & Sons.

Quintano, C., A. Fernández-Manso, and D.A. Roberts. 2013. Multiple Endmember Spectral Mixture Analysis (MESMA) to map burn severity levels from Landsat images in Mediterranean countries. *Remote Sensing of Environment* 136: 76–88. https://doi.org/10.1016/j.rse.2013.04.017.

Quintano, C., A. Fernández-Manso, and D.A. Roberts. 2020. Enhanced burn severity estimation using fine resolution ET and MESMA fraction images with machine learning algorithm. *Remote Sensing of Environment* 244: 111815. https://doi.org/10.1016/j.rse.2020.111815.

Quintano, C., L. Calvo, A. Fernández-Manso, S. Suárez-Seoane, P.M. Fernandes, and J.M. Fernández-Guisuraga. 2023. First evaluation of fire severity retrieval from PRISMA hyperspectral data. *Remote Sensing of Environment* 295: 113670. https://doi.org/10.1016/j.rse.2023.113670.

R Core Team. 2023. *R: A language and environment for statistical computing*. R Foundation for Statistical Computing. https://www.r-project.org/.

Riaño, D., E. Chuvieco, J. Salas, A. Palacios-Orueta, and A. Bastarrika. 2002. Generation of fuel type maps from Landsat TM images and ancillary data in Mediterranean ecosystems. *Canadian Journal of Forest Research* 32 (7): 1301–1315. https://doi.org/10.1139/x02-052.

Roberts, D.A., M. Gardner, R. Church, S. Ustin, G. Scheer, and R.O. Green. 1998. Mapping Chaparral in the Santa Monica Mountains Using Multiple Endmember Spectral Mixture Models. *Remote Sensing of Environment* 65 (3): 267–279. https://doi.org/10.1016/s0034-4257(98)00037-6.

Roberts, D.A., P.E. Dennison, M.E. Gardner, Y. Hetzel, S.L. Ustin, and C.T. Lee. 2003. Evaluation of the potential of Hyperion for fire danger assessment by comparison to the airborne visible/infrared imaging spectrometer. *IEEE Transactions on Geoscience and Remote Sensing* 41 (6): 1297–1310. https://doi.org/10.1109/tgrs.2003.812904.

Roberts, D., K. Halligan, P. Dennison, K. Dudley, B. Somers and A. Crabbe. 2019. *VIPER Tools User Manual*. [User's Manual].

Roth, K.L., P.E. Dennison, and D.A. Roberts. 2012. Comparing endmember selection techniques for accurate mapping of plant species and land cover using imaging spectrometer data. *Remote Sensing of Environment* 127: 139–152. https://doi.org/10.1016/j.rse.2012.08.03.

Rothermel, Richard C. 1972. A mathematical model for predicting fire spread in wildland fuels. Res. Pap. INT-115. Ogden, UT: U.S. Department of Agriculture, Intermountain Forest and Range Experiment Station. 40 p.

Roussel, J.R., D. Auty, N.C. Coops, P. Tompalski, T.R.H. Goodbody, A.S. Meador, J.F. Bourdon, F. de Boissieu, and A. Achim. 2020. lidR: An R package for analysis of Airborne Laser Scanning (ALS) data. *Remote Sensing of Environment* 251: 112061. https://doi.org/10.1016/j.rse.2020.112061.

Saarela, S., S. Holm, S.P. Healey, H.-E. Andersen, H. Petersson, W. Prentius, P.L. Patterson, E. Næsset, T.G. Gregoire, and G. Ståhl. 2018. Generalized Hierarchical Model-Based Estimation for Aboveground Biomass Assessment Using GEDI and Landsat Data. *Remote Sensing* 10 (11): 1832. https://doi.org/10.3390/rs10111832.

Saatchi, S., K. Halligan, D.G. Despain, and R.L. Crabtree. 2007. Estimation of forest fuel load from radar remote sensing. *IEEE Transactions on Geoscience and Remote Sensing* 45 (6): 1726–1740. https://doi.org/10.1109/tgrs.2006.887002.

Sankey, T.T., J. McVay, T.L. Swetnam, M.P. McClaran, P. Heilman, and M. Nichols. 2018. UAV Hyperspectral and LiDAR Data and Their Fusion for Arid and Semi-Arid Land Vegetation Monitoring. *Remote Sensing in Ecology and Conservation* 4: 20–33. https://doi.org/10.1002/rse2.44.

San-Miguel-Ayanz, J., J.M. Moreno, and A. Camia. 2013. Analysis of large fires in European Mediterranean landscapes: Lessons learned and perspectives. *Forest Ecology and Management* 294: 11–22. https://doi.org/10.1016/j.foreco.2012.10.050.

Scott, J. H., and R.E. Burgan. 2005. Standard fire behavior fuel models: a comprehensive set for use with Rothermel's surface fire spread model. USDA Forest Service, Rocky Mountain Research Station, General Technical Report RMRS-GTR-153.

Settle, J., and N. Campbell. 1998. On the errors of two estimators of sub-pixel fractional cover when mixing is linear. *IEEE Transactions on Geoscience and Remote Sensing* 36 (1): 163–170. https://doi.org/10.1109/36.655326.

Solares-Canal, A., L. Alonso, T. Rincón, J. Picos, D.M. Molina-Terrén, C. Becerra, and J. Armesto. 2023. Operational fuel model map for Atlantic landscapes using ALS and Sentinel-2 images. *Fire Ecology* 19 (1): 1–25. https://doi.org/10.1186/s42408-023-00218-y.

Speiser, J.L., M.E. Miller, J. Tooze, and E. Ip. 2019. A comparison of random forest variable selection methods for classification prediction modeling. *Expert Systems with Applications* 134: 93–101. https://doi.org/10.1016/j.eswa.2019.05.028.

Tanase, M.A., M. Santoro, C. Aponte, and J. de la Riva. 2014. Polarimetric Properties of Burned Forest Areas at C- and L-Band. *IEEE Journal of Selected Topics in Applied Earth Observations and Remote Sensing* 7: 267–276. https://doi.org/10.1109/JSTARS.2013.2261053.

Valbuena, R., M. Maltamo, L. Mehtätalo, and P. Packalen. 2017. Key structural features of Boreal forests may be detected directly using L-moments from airborne lidar data. *Remote Sensing of Environment* 194: 437–446. https://doi.org/10.1016/j.rse.2016.10.024.

Van Ewijk, K. Y., P. M. Treitz, and N. A. Scott. 2011. Characterizing Forest Succession in Central Ontario using Lidar-derived Indices. *Photogrammetric Engineering and Remote Sensing* 77 (3): 261–269. https://doi.org/10.14358/pers.77.3.261.

Van Wagner, C. E., B. J. Stocks, B. D. Lawson, M. E. Alexander, T. J. Lynham, and R. S. McAlpine. 1992. *Development and structure of the Canadian forest fire behavior prediction system*. Forestry Canada Fire Danger Group. Information Report *ST-X-3*..

Viedma, O., F. Chico, J. J. Fernández, C. Madrigal, H. D. Safford, and J. M. Moreno. 2020. Disentangling the role of prefire vegetation vs. burning conditions on fire severity in a large forest fire in SE Spain. *Remote Sensing of Environment* 247: 111891. https://doi.org/10.1016/j.rse.2020.111891.

Viedma, O., C.A. Silva, J.M. Moreno, and A.T. Hudak. 2024. LadderFuelsR: A new automated tool for vertical fuel continuity analysis and crown base height detection using light detection and ranging. *Methods in Ecology and Evolution* 15 (11): 1958–1967. https://doi.org/10.1111/2041-210x.14427.

Wang, J., R. Lopez-Lozano, M. Weiss, S. Buis, W. Li, S. Liu, F. Baret, and J. Zhang. 2022. Crop specific inversion of PROSAIL to retrieve green area index (GAI) from several decametric satellites using a Bayesian framework. *Remote Sensing of Environment* 278: 113085. https://doi.org/10.1016/j.rse.2022.113085.

Woods, M., K. Lim, and P. Treitz. 2011. Predicting forest stand variables from LiDAR data in the Great Lakes-St. Lawrence forest of Ontario. *The Forestry Chronicle* 84 (6): 827–839. https://doi.org/10.5558/tfc84827-6.

Woolley, T. 2016. *LiDAR Derived Data to Inform Vegetative Structural Conditions*. Flagstaff, Arizona.

Yebra, M., and E. Chuvieco. 2009. Linking ecological information and radiative transfer models to estimate fuel moisture content in the Mediterranean region of Spain: Solving the ill-posed inverse problem. *Remote Sensing of Environment* 113 (11): 2403–2411. https://doi.org/10.1016/j.rse.2009.07.001.

Zhang, K., S.C. Chen, D. Whitman, M.L. Shyu, J. Yan, and C. Zhang. 2003. A progressive morphological filter for removing nonground measurements from airborne LIDAR data. *IEEE Transactions on Geoscience and Remote Sensing* 41 (4): 872–882. https://doi.org/10.1109/tgrs.2003.810682.

Zhang, J., J. Hu, J. Lian, Z. Fan, X. Ouyang, and W. Ye. 2016. Seeing the forest from drones: Testing the potential of lightweight drones as a tool for long-term forest monitoring. *Biological Conservation* 198: 60–69. https://doi.org/10.1016/j.biocon.2016.03.027.

Publisher's Note